

Mesostructured hybrid organic–inorganic thin films

Lionel Nicole, Cédric Boissière, David Grosso, Alida Quach and Clément Sanchez*

Received 29th April 2005, Accepted 8th July 2005

First published as an Advance Article on the web 3rd August 2005

DOI: 10.1039/b506072a

This review discussed the design and different synthetic routes that lead to hybrid thin films that have a periodically organised porosity. The mechanism of formation, the role of the organic functionality and the resulting mesophase, the comparison between one-pot and post-synthesis approaches and the applications domain of this mesostructured hybrid film are described and discussed in this article.

1 Introduction

The concept of “hybrid organic–inorganic” nanocomposites exploded in the eighties with the expansion of soft inorganic chemistry processes.^{1–4} Indeed, the very high adaptability of the sol–gel process (salts or metallo-organic precursors, aqueous or organic solvents, low processing temperatures,

processing versatility of the colloidal state) allow the mixing of inorganic and organic components at the nanometric scale, in virtually any ratio, leading to the so-called hybrid organic–inorganic nanocomposites.^{5–14}

Since the development of organic templated growth of inorganic materials in the nineties, the elaboration of new types of porous hybrid materials whose structure and function are organised hierarchically is emerging.^{15,16} Ordered periodic micro-, meso- and macroporous materials allow the construction of composites with many guest types, e.g. organic molecules, inorganic ions, semiconductor clusters or polymers.

Laboratoire de Chimie de la Matière Condensée (CNRS UMR 7574), Université Pierre et Marie Curie, 4 Place Jussieu, 75252 Paris cedex 05, France. E-mail: clems@ccr.jussieu.fr; Fax: 33 (0)1 4427 4769; Tel: 33 (0)1 4427 3365



Lionel Nicole

Lionel Nicole (born 30/09/1973 in France) obtained his Ph.D. in 2002 on “organic–inorganic mesoporous materials applied to encapsulation–sorption processes” (Montpellier, France). After one year in a post-doctoral position in Clément Sanchez’ group and one year in Professor MacCraith’s laboratory (Dublin), he obtained an assistant professor position at the “Laboratoire CMC”.



Cédric Boissière

Cédric Boissière (born 03/04/1974 in France) obtained his Ph.D. in 2001 for his work on “inorganic mesostructured materials applied to separation processes” at the European Institute of Membranes (Montpellier). After one year in a postdoctoral position in Professor Stephen Mann’s group at Bristol (UK), he obtained a CNRS researcher position at the “Laboratoire CMC” in 2002 for developing new approaches of hierarchical hybrid materials.



David Grosso

David Grosso (35 years old) obtained his Ph.D. in 1999 on Optical Coatings (University of Surrey, UK). For the past 4 years, he has been an assistant professor at the University of Paris. His present interests concern self assembly of mesoporous materials. He is co-author of about 55 publications and has presented 6 invited lectures at international conferences.



Alida Quach

Alida Quach is doing a doctoral thesis at the University Pierre et Marie Curie in Paris. Her present interest concerns the design and characterization of hybrid functional thin films, especially optical sensors for heavy metal detection.

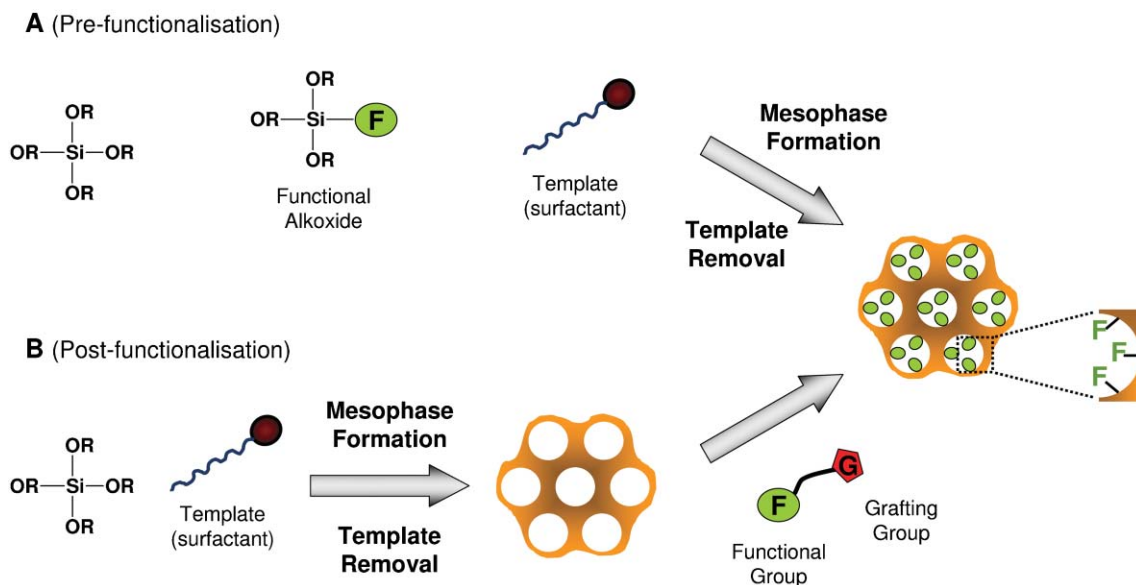


Fig. 1 Pre-functionalisation (A) and post-functionalisation (B) routes towards hybrid materials organised in the mesoscopic scale. The meso-organised precursors are synthesised by reacting an inorganic precursor in the presence of a supramolecular template (surfactant). By route A, organic functions can also be embedded within the walls. Adapted from reference 15.

These guest/host materials combine high stability of the inorganic host, new structure forming mechanisms due to the confinement of guests in well defined pores, and a modular composition.

Chemical functionalisation of the inorganic framework of porous materials, for example through the covalent coupling of organic or organo-metallic moieties, is a promising approach to tailor pore surface properties such as hydrophobicity, polarity, and catalytic, optical and electronic activity.^{17–19} Indeed, the tuning of the pore surface chemistry is of direct interest in applications such as catalysis, chromatography, controlled delivery or membranes. Organo-functionalisation of ordered mesoporous silica-based solids can be achieved either by post-synthetic methods^{20–24} or *via* direct routes (one-pot synthesis)^{25–34} (Fig. 1). The latter involves

co-condensation of tetraalkoxysilanes and organotrialkoxysilanes in the presence of surfactants. The one-pot synthesis method allows a higher organic content and a more homogeneous organic distribution in the material.³⁵ Numerous studies have highlighted the role and importance of the nature of the bonds constituting the hybrid inorganic–organic interface. Hybrid materials with covalently bonded organic moieties (Class II hybrids⁵) can be readily designed by sol-gel chemistry and thus a wide range of materials with tailor-made structure and properties can be reproducibly prepared.

This article reviews the research performed in the field of hybrid organic–inorganic films, which present periodically organised mesoporosity. Emphasis will be given to the two different grafting methods, in particular the more commonly employed “one-pot” synthesis, in terms of localisation and



Clément Sanchez

He is currently performing research at the University Pierre and Marie Curie in Paris. He was professor at l'Ecole Polytechnique (Palaiseau) from 1991 to 2003. He currently leads a research group of ten scientists and he specialises in the field of chemistry

Clément Sanchez is Director of Research at the French Research Council (CNRS) and Director of the Laboratoire de Chimie de la Matière Condensée at the University Pierre and Marie Curie of Paris. He received an engineering degree from l'Ecole Nationale Supérieure de Chimie de Paris in 1978 and a thèse d'état (Ph.D.) in physical chemistry from the University of Paris VI in 1981. He did post-doctoral work at the University of California, Berkeley, and is

and physical properties of nanostructured porous and non-porous transition metal oxide based gels and porous and non-porous hybrid organic–inorganic materials shaped as monoliths, microspheres and films. He received the French IBM award for materials science in 1988 and was a recipient of the Société Chimique de France award for solid state chemistry in 1994. He was the recipient of the Silver Medal of the CNRS for chemistry in 1995 and he also received an award of the French Academy of Sciences for Application of Science to Industry in 2000. He has organised several international meetings associated with the fields of soft chemistry, hybrid materials and related bio-aspects: the First European Meeting on Hybrid Materials (1993); five Materials Research Symposia: Better Ceramics Through Chemistry VI (1994), Hybrid Organic–Inorganic Materials B.T.C. VII (1996), and Hybrid Materials (1998 and 2000, 2004); three EUROMAT 2003 Symposia and one E-MRS 2005. He is also a member of the Materials Research Society and the Société Chimique de France. He is the author of over 250 scientific publications, co-editor of 9 books or proceedings related to hybrid materials and more than 20 patents. He has also presented over 60 invited lectures at international meetings.

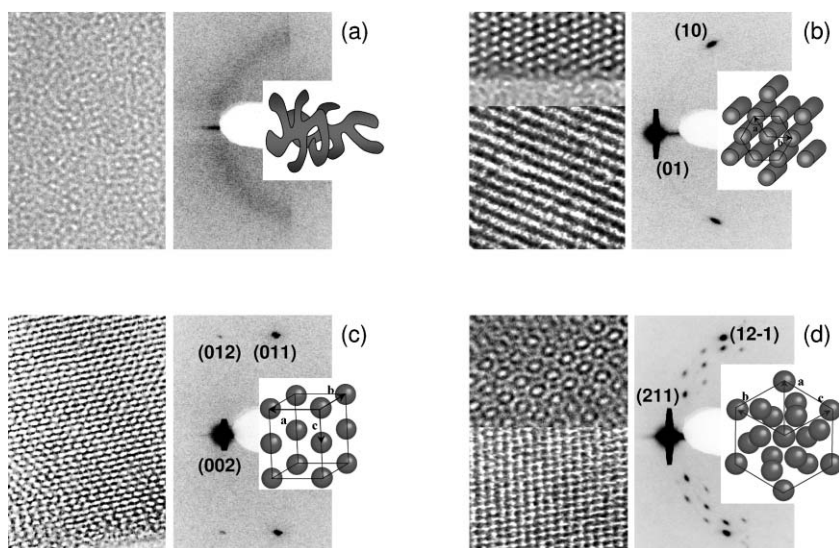


Fig. 2 2D SAXS patterns corresponding to the various types of mesostructures obtained (right). Lattice models of similar symmetry group and typical TEM images representing various cutting directions (left). (a) Worm-like, (b) 2D hexagonal ($p6m$ space group), (c) 3D hexagonal ($P6_3/mmc$ space group), (d) cubic ($Pm\bar{3}n$ space group). Adapted from reference 67.

effects of organosilane species on the mesostructuration. The first part of the review deals with the general background of mesoporous thin films. In the second part, the two different functionalisation routes are discussed and finally, applications concerning optical sensors, low k dielectrics, photonics, microvalves and microfluidics are highlighted.

2 Background of mesoporous thin films

2.1 General background

Among the various shapes and morphologies of such mesoporous materials (powders, monoliths, fibers, films, *etc.*), thin films have shown a morphology suitable for applications in optical, electronic, and sensing devices, as well as separation,³⁶ mainly due to the versatility of coating on various substrates and commercial supports such as optical fibres.

Mesoporous thin films can be prepared by several methods:

- Self-standing silica films produced at air–water^{37–41} and oil interfaces,⁴² resulting from the transport of material from the solution towards the interface. Films at the air–water interface are grown from a homogeneous solution of the reactants after hydrolysis in the water phase, while for growth of films at the oil–water interface, the water-insoluble silica source is positioned in the oil phase.

- The first generation of supported mesoporous silica films was reported in 1996.^{43–45} Typically, substrates were introduced into silica/surfactant/solvent systems used to prepare bulk hexagonal mesophases (initial surfactant concentrations $c_0 >$ critical micelle concentration, cmc). Under these conditions, hexagonal silica–surfactant mesophases are nucleated on the substrate with pores oriented parallel to the substrate surface. Growth and coalescence over a period of hours to weeks resulted in continuous but macroscopically inhomogeneous films characterized by granular textures on micrometer-length scales.

In 1999, Brinker *et al.*⁴⁶ reported a new approach, which resulted in highly ordered mesostructured thin films, called “Evaporation Induced Self Assembly” (EISA). This synthesis route presents several advantages such as the versatility of processability, a short mesophase formation (a few minutes) and the fact that it gives access to a large variety of mesophases (Fig. 2). Starting with homogeneous hydro-alcoholic solutions of soluble silica sources (monomeric and oligomeric silicic acid species), surfactant (initial surfactant concentrations $c_0 \ll$ cmc) and, optionally, other organic and inorganic species, the preferential evaporation of alcohol that accompanies spin-coating,^{45–47} dip-coating,^{48–52} ink-jet printing,⁵³ aerosol deposition,⁵⁴ or selective dewetting⁵³ drives silica/surfactant self assembly⁵⁵ into uniform or spatially-patterned⁵³ thin-film mesophases. Through subsequent heating or exposure to catalysts or light,^{50,56} these films can be processed into porous^{45–51} or nanocomposite mesostructures^{52,57} of potential utility for a diverse range of applications such as sensors,^{58–60} membranes,⁶¹ catalysts, waveguides,⁶² lasers,⁶² nano-fluidic systems,⁵³ molecular valves^{63,64} and low dielectric constant (so-called low k) insulators.^{65,66} This EISA process^{46,67} is useful because it enables rapid, efficient integration of well-defined nanostructures into microelectronic devices and microsystems, using readily available processing methods. As most hybrid mesostructured and functionalised thin films have been synthesised by EISA⁴⁶ it is necessary to give a short overview of this pathway (for a complete understanding see, for example, the feature article by Grosso *et al.*⁶⁷).

2.2 Self assembly processes: EISA

In the published literature, two main processes have been proposed to explain the hybrid nano-organisation of inorganic structures with surfactants. The first is the liquid crystal templating (LCT) mechanism,^{55,68} in which the inorganic phase condenses around a stabilised surfactant mesophase. The second is the cooperative self-assembly

(CSA) mechanism^{67,69–76} in which surfactant molecules and inorganic species combine in a first step to form hybrid intermediate entities that behave as independent surfactant species—building blocks of hybrid structures. However, it is most likely that a combined effect of both mechanisms governs the synthesis of such hybrid materials, depending on the chemical and processing critical parameters for a given system.

These parameters can be divided into two families: first, the chemical factors that govern the relative quantity of surfactant and inorganic precursor and the kinetics of hydrolysis–condensation reactions; and second, the processing conditions that govern the diffusion of volatile EtOH, H₂O and HCl molecules into or out of the film, fixing the dry film composition and its final thickness. The preparation of reproducible mesoporous organised thin films with optical homogeneity and transparency requires the understanding and control of three main levels, namely, the chemistry associated with the initial solution, the processes linked to the layer deposition technique, and the thermal, washing or UV post-treatments. The main studies involve films prepared with the silica precursor tetraethylorthosilicate (TEOS), cetyltrimethylammonium bromide (CTAB) as surfactant, HCl as condensation catalyst, and water and alcohol as solvent.

2.2.1 Tuning the composition of the initial solution. In consideration of the above remarks, the optimal sols are composed of ethanol, for its high volatility, its high wettability properties with hydrophilic substrates, and its miscibility with the inorganic source (metal alkoxides, chloro alkoxides or metallic salts). In order to favour fast hydrolysis and slow condensation, which promotes the formation of small oligomers that one can control and stabilise in a small period of time, the pH is generally fixed close to the isoelectric point of the silica ($H^+/Si \approx 0.14\text{--}0.004$) while the hydrolysis ratio ($h = H_2O/Si$) is fixed at 5. Hydrochloric acid is the ideal acid because, after having fulfilled its catalytic role in the sol, its volatility facilitates its removal during film evaporation. The aging time of the sol has to be controlled since it was reported that the condensation degree of the inorganic oligomers can greatly influence the mesostructuration.^{71,77} The relative amounts of organic and inorganic (surfactant/inorganic precursors molar ratio) have to be reasonably fixed to permit the meso-organisation in the intermediate hybrid state and to be stable after removal of the template.⁶⁷

2.2.2 The film deposition step (EISA). The control of the initial sol is related to the chemical parameters, while the control at the deposition level is more related to process conditions. Here, by concentrating non-volatile species, evaporation is the driving force of the self-assembly process and the silica condensation. More precisely, as soon as a layer of the initial sol is deposited on the substrate, evaporation of volatile components (*e.g.* EtOH, H₂O, and HCl) takes place at the air/film interface. The evaporation leads to the progressive but rapid (10–30 s) enrichment of the film in silica oligomers and template molecules. In due course, when the surfactant concentration has reached the equivalent of the cmc for the

system,⁷⁸ micelles start to form by hydrophobic segregation of alkyl chains. An organised mesostructure is eventually formed, characterised by the physico-chemical properties of the surfactant molecules in the actual medium. Recently, the mechanism of self-assembly has been investigated by *in-situ* SAXS experiment. Details on intermediate phases and concentration gradient have been discussed.^{71,79} This powerful investigation tool was applied to study the influence of processing parameters, such as the relative humidity (RH) within the dip-coating chamber.⁸⁰ The data show that the final mesostructure is formed after the drying line, where one can consider the evaporation to be completed. In addition, it was demonstrated that for the same system, mono-dimensional to tri-dimensional mesophases can be formed by simply varying the relative humidity from 20 to 70% inside the cabinet during and after evaporation. Since all other parameters remain unchanged, it is likely that the quantity of water in the films varies with RH after the drying line and thus influences the final organisation. Since the final mesostructure is formed during this diffusion equilibration, where the mineral network is not too extensively condensed, this period is referred to as the Modulable Steady State (MSS), where one can select a mesostructure by varying the “atmospheric” composition (relative humidity). Therefore, the hybrid intermediate mesostructured film behaves as a Liquid Crystal (LC) phase, the morphology of which depends on the MSS medium composition. A scheme of mesostructured thin film deposition by evaporation and its various successive steps is depicted in Fig. 3. The EISA can thus be described by competitive processes related to kinetics of condensation *versus* kinetics of organisation, both influenced by the kinetics of volatile species diffusion. These processes are difficult to control and thus difficult to predict because they occur successively or simultaneously during drying. For a conventional CTAB/TEOS system, the MSS lasts from a few seconds at low humidity to 10 minutes at high humidity.⁸⁰ For transition metal oxide (TMO) based films prepared in highly acidic conditions to quench extended condensation, the MSS can last several hours.^{80–82}

2.2.3 The film post-treatment step. The aim of this step is the stabilisation of the inorganic network by further condensation and the liberation of the porosity through the template elimination. This is usually achieved by thermal decomposition of the organic phase and is always accompanied by a unidirectional contraction of the meso-domain normal to the surface plane.^{51,71,83,84} For TMO-based films, a mesoporous structure degradation is associated to the crystallisation of the network,⁸⁵ but can still be controlled to obtain pure crystalline mesoporous networks.^{82,86–88} On the other hand, structures obtained with the present TEOS/CTAB system are stable up to 800 °C.⁷⁷ Also cyclic and branched silica oligomers, which compose the film, are stable up to 400 °C and collapse after this temperature without noticeably perturbing the mesoporosity. Some proposed mild treatments exploit the fact that, in such acidic conditions, silica and CTAB are in $S^+X^-I^+$ type ionic interaction ($CTA^+ Br^- + H_2O-Si$),⁷³ and that CTAB thermally decomposed around 300 °C. It is possible to combine mild temperature treatment, basic treatment (NH₃

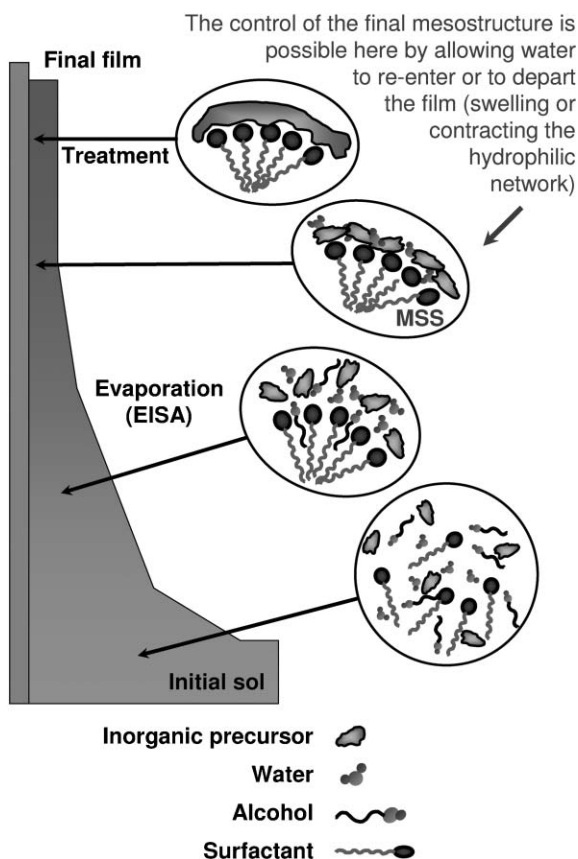


Fig. 3 Mesostructured thin film formation by dip-coating. Step 1: the isotropic initial sol, where the condensation is optimally slowed down. Step 2: the evaporation proceeds and micelles start to form above the cmc. Step 3: the evaporation is complete; the film equilibrates with its environment (MSS) and the final mesostructure is selected by adjusting the RH before further inorganic condensation. Step 4: the inorganic network is condensed; the hybrid mesostructure is stabilised. Adapted from reference 67.

atmosphere),⁵¹ solvent extraction^{51,56,89} and degradation of organics by UV-O₃.⁵⁶ There is, therefore, a great variety of possible treatments that can be adapted to the type of material and to the targeted application.

2.2.4 Resulting mesophases and modulable steady state. Thus, the final structure depends mainly on three critical parameters, namely the surfactant/inorganic precursor molar ratio, the chemical nature of the inorganic precursor, and the relative humidity in which the evaporation takes place (Fig. 4). The first parameter is fixed during the preparation and the second parameter is controlled by the sol-gel chemistry conditions. The effect of the third parameter is more delicate to interpret because it acts at several levels on various secondary phenomena (viscosity, condensation, *etc.*). A crucial period of time referred to as the Modulable Steady State (MSS) occurs just after the evaporation. During this time the film water and solvent contents are in equilibrium with the environment and the final structure is defined and stabilised. In other words, the final mesostructure formed depends on the nature and relative composition of the chemical species present in the film during the MSS. The pseudo phase diagram of the [SiO_x(OH)_y-H₂O-EtOH-CTAB] system is given as an example in Fig. 4. Considering non-silicates species, similar work was reported for the [TiO₂-H₂O-EtOH-F127] system.^{67,82,90}

3 Grafting methods

The addition of organic groups by post-synthetic grafting of R_xSi(OR')_{3-x}, R_xSiCl_{4-x} onto the surface of the pores results in functional mesoporous inorganic-organic hybrid materials offering a further possibility to tailor the chemical properties of the porous materials. This post-synthetic grafting process has been widely employed to anchor various organic groups onto the surface of the pores, including organometallic species, amino and thiol groups, and epoxide functions. However, this method often leads to a quite low loading, an inhomogeneous distribution of the functional groups, and a decrease of the pore volume.¹⁸ The alternative route of applying organosiloxanes directly during the synthesis by co-condensing them with tetraalkoxysilanes leads to a higher loading but above a limit of around 25% RSiO₃ groups the mesostructure generally collapses. Functional groups, such as vinyl,^{28,35} 3-sulfanylpropyl,^{26,91} phenyl,²⁵ aminopropyl,^{26,27} cyanoethyl²⁷ and diphenylphosphanylpropyl,⁹² have been incorporated by this method into the inorganic network. Recently, based on this

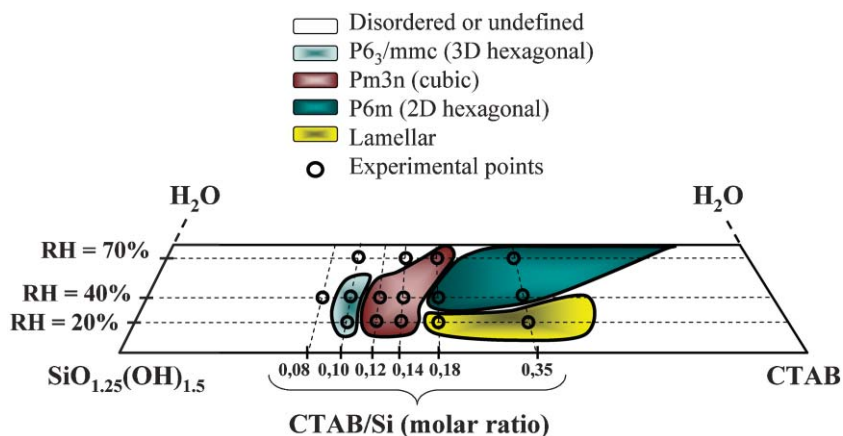


Fig. 4 The diagram of textures of MSS period depending on chemical (aging time and sol composition) and process parameters (relative humidity), established for CTAB/SiO_{1.25}(OH)_{1.5}/EtOH/H₂O system (in %). Adapted from reference 67.

approach, amphiphiles with a cleavable alkyl chain and a condensable head group were used as templates for the synthesis of mesoporous silica materials.⁹³ After the synthesis, the cleavage and removal of the alkyl chains left nanopores with a densely functionalised surface.

An expansion of the above mentioned concepts was the incorporation of bifunctional organosiloxane precursors, also referred to as bridged silsesquioxanes, of the general formula $[(R'O)_3Si]_mR$ ($m \geq 2$) as the network forming species.³³ The resulting materials, called periodic mesoporous organosilicas (PMOs), contain the organic groups as an integral part of the inorganic-oxide framework and the inorganic and organic moieties are covalently linked to each other. They will be discussed in detail in other feature articles appearing in this special issue.

3.1 Co-condensation or “one-pot” synthesis

The main data concerning one-pot synthesis of mesoporous thin films are gathered in Table 1. the organometallic precursor, the surfactant and experimental conditions, the nature of the mesophase, the targeted applications and the references are reported.

The one-pot synthesis presents several advantages compared to post-grafting: (i) the functionalisation and structuring of films take place at the same time, (ii) it generally induces a homogeneous distribution of organic probes within the network and (iii) the stoichiometry of the thin film is perfectly controlled and is equal to the composition of the initial solution. However, several difficulties, which will be developed in the following sections, exist in addition to the control of the main parameters related to the EISA process:

- Solubilisation of the probes (organic functionalities) in the medium (addition of co-solvent or protonation).
- Chemical reactions in the organic domain (polymerisation of organic species).
- Localisation of the probes (organic, inorganic regions or interface).
- Control of the mesophase (influence of the nature and/or amount of probes on the final mesophase).
- In some cases the organic functionalities can not be stable in the conditions of one-pot synthesis (*i.e.* some phosphines, *etc.*).

3.1.1 Influence of chemical and processing parameters (EISA parameters). Even if silylated probes have an influence on the mesostructuration, as we will see later, the main parameters of EISA are always crucial. The influence of pH, aging time of sol and ethanol vapour concentration during dip-coating on the final mesostructure of $[\text{SiO}_2\text{-CTAB}]$ functionalised thin films have been studied carefully by replacing of 20% mol of the starting precursor tetraethoxysilane (TEOS) by methyl- or phenyltriethoxysilane (MTES or PTES).^{94–96}

Aging time of the sol. Chemical composition of the films and aging of the precursors direct final mesostructures. For functionalised films containing 20% mol of organosilica,^{94,95} the 3D hexagonal phase is generally obtained with sols aged between 2 and 24 h, whereas the cubic phase appears

afterwards with sols aged between 24 and 72 h. At longer aging times, less organised phases are formed. In the absence of organic groups for pure silica, similar 3D phases are observed but for longer aging times, and with larger measured cell parameters (5–15 Å). Similar results were also observed by de Theije *et al.*⁹⁶

pH of the sol. For low-acidified sols (aqueous HCl 10^{-2} M solution),^{94,95} only the formation of a 2D hexagonal mesophase (plane group $p6m$) is observed. For acidity (HCl 10^{-1} M), different behaviours are noticed. Short aging times of the sols (from 2 to 24 h) always lead to a 3D hexagonal mesophase (space group $P6_3/mmc$) whereas, for longer aging times of the sols, and depending on dip-coating conditions, either the previous mesophase (low concentration in ethanol vapour—*vide infra*) or a cubic mesophase ($Pm3n$) (high concentration in ethanol vapour) are obtained.

Relative humidity and ethanol vapour. By changing the dip-coating conditions (relative humidity, water, ethanol), hybrid films with different mesostructures are formed from identical sols.^{94,95} For the same-aged sols, films containing phenyl groups are obtained with a 3D hexagonal phase for a humidity under 40% RH inside the open dip-coater. Increasing humidity up to 55% RH favours the formation of the cubic phase, but the 3D hexagonal phase may also be observed. In addition, confinement and increased ethanol vapour content (from less than 0.2% in volume to 1% and more) at moderate humidity (40% RH) are needed in order to isolate the cubic phase. This sensitivity to dip-coating conditions is related to water and ethanol concentrations in air that greatly influence their concentrations in the film even after passing the drying line. In some cases, this favours a hexagonal ($P6_3/mmc$) \rightarrow cubic ($Pm3n$) phase transition like the one observed during the deposition of silica films.⁷¹

Chemical composition of the starting sol. Jung *et al.*⁹⁷ observed with films containing 10% mol of 3,3,3-trifluoropropyltrimethoxysilane that the final mesophase structure is a function of the surfactant/silica ratio. At a surfactant to organosilane mole ratio of approximately 0.17, the predominant phase was a hexagonal mesostructure. However, at a surfactant to organosilane molar ratio of approximately 0.13, a cubic phase was produced. These changes in mesostructure with surfactant concentration are in agreement with the mesophase diagram established for silica.⁶⁷ However, it has been shown in several studies that the nature of the silylated probe and its amount in thin films also greatly influence the final mesostructure.^{60,98,99}

3.1.2 Solubilisation of the organofunctional molecules in the medium. The EISA method, which is used in almost all the syntheses of functionalised and mesostructured silica thin films, implies a homogeneous starting sol. However, when the silylated probe is poorly soluble or insoluble in the alcoholic sol, segregation or aggregation can take place. This phenomenon maybe due to an insufficient hydrolysis of the organosilane precursor, resulting in hydrophobic species. In some cases, the precursor can be insoluble regardless of the

Table 1 Functional organosilanes and properties of resultant thin film mesophases

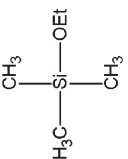
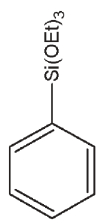
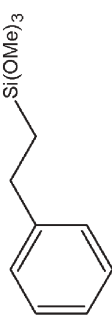
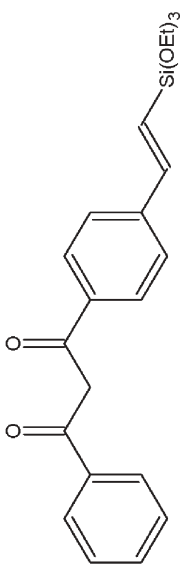


Functional organosilanes	Experimental conditions and results	Properties/applications and references
1) Methyltriethoxysilane, ^{94,95,104,147} Propyltrimethoxysilane ⁹⁸	CTAB, F/TEOS = 0.25; 2D hex, 3D hex, cubic CTAB, F/TEOS = 0.11–0.43; 2D hex PS(35)- <i>b</i> -PEO(109); cubic CTAB, F/TEOS = 0.15; 2D hex	— ^{94,95} Low- <i>k</i> dielectric materials ¹⁴⁷ — ¹⁰⁴ Separation, catalysis, sensing ⁹⁸
H ₃ C—Si(OEt) ₃ H ₃ C—CH ₂ —CH ₂ —Si(OMe) ₃		
2) Trimethylethoxysilane	TEOS, CTAB; 2D hex post-grafting	Low- <i>k</i> dielectric materials ¹⁴⁷
		
3) Phenyltriethoxysilane	CTAB, F/TEOS = 0.25; 2D hex, 3D hex, cubic CTAB, F/TEOS = 0–0.15; cubic	— ^{94,95} Separation, catalysis, sensing ⁹⁸ — ¹¹³
		
4) (2-Phenylethyl)trimethoxysilane	CTAB F/TEOS = 0–0.02; cubic F/TEOS = 0.02–0.15; 2D hex	Separation, catalysis, sensing ⁹⁸
		
5) Triethoxydibenzoylmethane	CTAB F/TEOS = 0–0.01; cubic F/TEOS = 0.027–0.053; 2D hex F/TEOS > 0.053; lamellar	Heavy metals sensor ⁶⁰
		
6) Aminopropyltrimethoxysilane	Brij-56/CTAB, F/TEOS = 0.039–0.08; cubic CTAB, F/TEOS = 0.15; 2D hex (acidic form) Brij 56, F/TEOS = 0.25; cubic TEOS, CTAB; cubic post-grafting	Coupling of noble metals, dyes, and bioactive molecules ^{53,124} Separation, catalysis, sensing ⁹⁸ Receptors for biomolecules ¹⁰⁵ Sorption of heavy metals, coupling additional functionality ¹⁴⁶ — ¹¹³
		
7) 3-(2-Aminoethylamino)propyltrimethoxysilane	TEOS, CTAB; cubic post-grafting	Sorption of heavy metals, coupling additional functionality ¹⁴⁶
		

Table 1 Functional organosilanes and properties of resultant thin film mesophases (*Continued*)

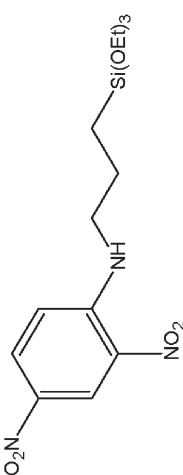
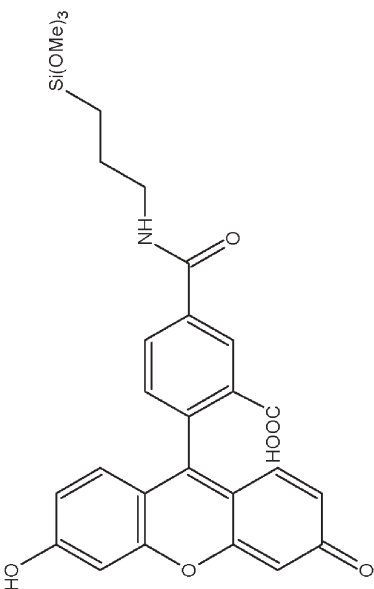
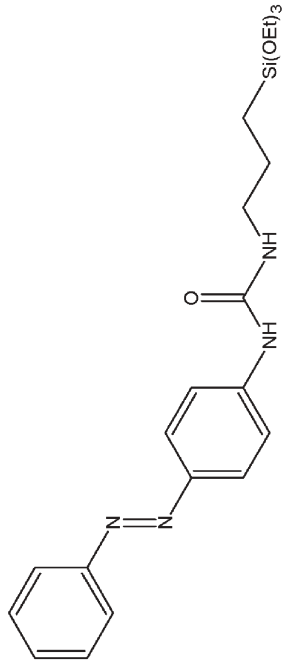
Functional organosilanes	Experimental conditions and results	Properties/applications and references
<p>8) 3-(2,4-Dinitrophenylamino)propyltriethoxysilane</p> 	<p>Brij-56/CTAB, F/TEOS = 0.039–0.08; 3D hex CTAB, F/TEOS = 0.15; 2D hex (acidic form) CTAB, F/TEOS = 0.11; 2D hex</p>	<p>Chromophore, nonlinear optical materials (χ^2)^{53,124} Separation, catalysis, sensing⁹⁸ Improved mechanical properties¹²⁶</p>
<p>9) Dye-NH(CH₂)₃-Si(OCH₃)₃; Dye = 5,6-carboxyfluorecein, succinimide ester (5,6-FAM, SE)</p> 	<p>Brij-56/CTAB, F/TEOS = 0.039–0.08; cubic</p>	<p>pH sensitive^{53,124}</p>
<p>10) 4-(3-Triethoxysilylpropylureido)azobenzene</p> 	<p>Brij 56, F/TEOS = 0.125; cubic</p>	<p>Smart gas masks, membranes, controlled release systems, externally controlled micro/nanofluidic-channel systems^{63,64}</p>

Table 1 Functional organosilanes and properties of resultant thin film mesophases (*Continued*)

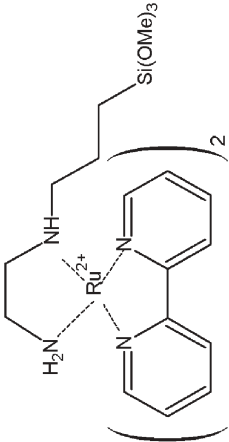

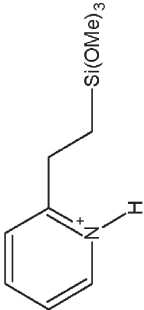
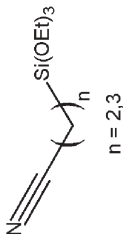

Functional organosilanes	Experimental conditions and results	Properties/applications and references
11) Ru(II) 2,2'-bipyridyl-2-aminoethyl-2-aminopropyltrimethoxysilane	106 107	
		
12) N-(3-Trimethoxysilylpropyl)pyrrole	CTAB, F/TEOS = 0–0.015; cubic	Separation, catalysis, sensing ⁹⁸
		
13) 2-(Trimethoxysilyl)ethylpyridine	CTAB, F/TEOS = 0.15; 2D hex	Separation, catalysis, sensing ⁹⁸
		
14) Cyanoalkyltriethoxysilane	Brij 56, F/TEOS = 0.28; cubic CTAB F/TEOS = 0–0.18; 2D hex F/TEOS > 0.18; worm-like	Receptors for biomolecules ¹²³ Easily hydrolysed to –COOH groups ⁹⁹
		
15) Isocyanatopropyltriethoxysilane	CTAB, F/TEOS = 0.15; 2D hex	Separation, catalysis, sensing ⁹⁸
		

Table 1 Functional organosilanes and properties of resultant thin film mesophases (*Continued*)

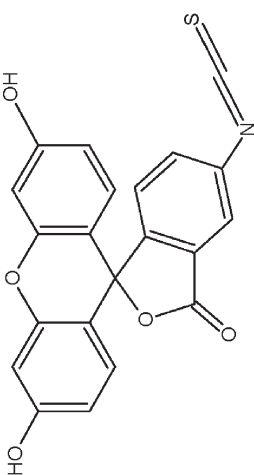
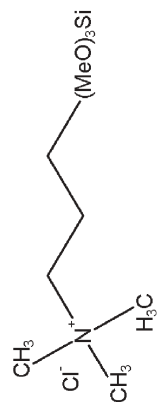
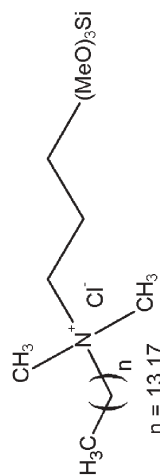
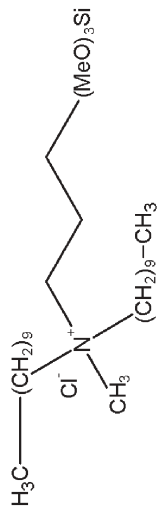
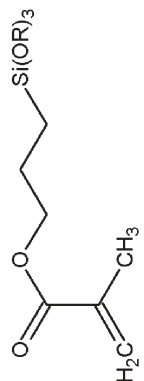
Functional organosilanes	Experimental conditions and results	Properties/applications and references
16) Fluorescein isothiocyanate (derivatized with APTS)	F127, F/TEOS = 4.4×10^{-4} ; 3D hex, cubic	Optical solid-state pH sensors ⁵⁹
		
17) <i>N</i> -Trimethoxysilylpropyl- <i>N,N,N</i> -trimethylammonium chloride	P123, F/BTSE = 0.025; 2D hex, 2D cubic	Molecular imprinting and selective binding of organophosphonate complexes ^{112,122}
		
18) Alkyl(dimethyl-(3-trimethoxysilylpropyl)ammonium chloride	P123, F/BTSE = 0.025; 2D hex	Molecular imprinting and selective binding of organophosphonate complexes ¹¹²
		
19) <i>N,N</i> -Didecyl- <i>N</i> -methyl-(3-trimethoxysilylpropyl)ammonium chloride	P123, F/BTSE = 0.025; 2D hex	Molecular imprinting and selective binding of organophosphonate complexes ¹²
		
20) Methacryloxypropyltrialkoxysilane	CTAB, F/TEOS = 0.15; 2D hex CTAB, F/TEOS = 0.1; lamellar (distorted)	Separation, catalysis, sensing ⁹⁸ Coupling agent with polymers ¹⁰¹
		

Table 1 Functional organosilanes and properties of resultant thin film mesophases (*Continued*)



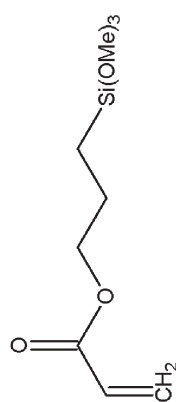




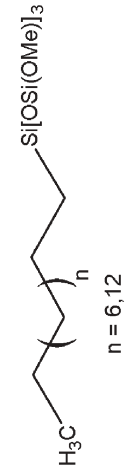
Functional organosilanes	Experimental conditions and results	Properties/applications and references
21) Vinyltrimethoxysilane, ¹⁵⁸ 7-octenyltrimethoxysilane  	CTAC; 2D hex CTAB, F/TEOS = 0.16; lamellar CTAB, F/TEOS = 0.08; lamellar	Catalyst support, separation ¹⁵⁸ Controlled release, membranes with switchable permeabilities ¹²⁸ Coupling agent with polymers ¹⁰¹
22) 3-(Trimethoxysilyl)propyl acrylate 	CTAB, F/TEOS = 0.16; lamellar (distorted)	Coupling agent with polymers ¹⁰¹
23) Perfluoroalkylsilane 	Brij-56/CTAB, F/TEOS = 0.039–0.08; 3D hex CTACl, F/TEOS = 0.11; cubic, 2D hex	Hydrophobic, low- <i>k</i> dielectrics ^{53,124} Optical devices, low- <i>k</i> dielectrics ⁹⁷
24) (Diphenylphosphine)propyltriethoxysilane 	CTAB, F/TEOS = 0.15; 2D hex	Separation, catalysis, sensing ⁹⁸
25) Mercaptopropyltrimethoxysilane 	Brij 56, CTAB, F/TEOS = 0.039–0.08; 3D hex CTAB, F/TEOS = 0.15; 2D hex TEOS, CTAB; cubic post-grafting TEOS, F127; cubic post-grafting	Coupling of noble metals ^{53,124} Separation, catalysis, sensing ⁹⁸ Sorption of heavy metals, coupling additional functionality ¹⁴⁶ Electrode sensing layer ¹⁴⁹ — ¹¹³
26) 3-Chloropropyltriethoxysilane 	CTAB F/TEOS < 0.05, > 0.18; 2D hex F/TEOS = 0.11–0.18; cubic	Easily substituted by chelating groups ⁹⁹
27) Alkylsiloxane oligomers 	No surfactant; 2D hex, lamellar	159

Table 1 Functional organosilanes and properties of resultant thin film mesophases (*Continued*)

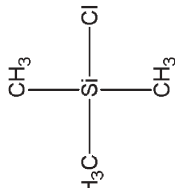


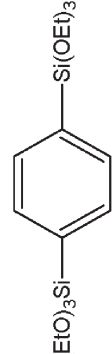
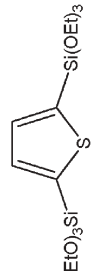
Functional organosilanes	Experimental conditions and results	Properties/applications and references
28) Trimethylchlorosilane 	P123, F/TEOS = 0.02–0.2; no structure	Hydrophobicity, integration into advanced semiconductor manufacture ¹²⁵
29) Bis(trialkoxysilyl)alkane  $n = 2, 3, 6, 8, 10$	Brij-56, CTAB, F/TEOS = 0.039–0.08; cubic CTAB/Brij 56/SDS/P123; lamellar, cubic, 2D hex $C_{12}H_{25}(EO)_{10}H$	Low- k dielectrics ^{53,124} Low- k dielectrics ³¹ Catalytic, separation ¹¹¹
30) Bis(triethoxysilyl)ethene, ³¹ bis(trialkoxysilyl)butene ¹¹¹ 	CTAB/Brij 56/SDS/P123; lamellar, cubic, 2D hex $C_{12}H_{25}(EO)_{10}H$; 3D hex	Low- k dielectrics ³¹ Catalytic, separation, and optical applications ¹¹¹
31) 1,4-Bis(triethoxysilyl)benzene 	$C_{12}H_{25}(EO)_{10}H$ CTAB/Brij 56/SDS/P123; lamellar, cubic, 2D hex	Catalytic, separation, and optical applications ¹¹¹ Low- k dielectrics ³¹
32) 2,5-Bis(triethoxysilyl)thiophene 	$C_{12}H_{25}(EO)_{10}H$; 3D hex	Catalytic, separation, and optical applications ¹¹¹
33) Hexamethyldisilazane $(Me)_3Si-NH-Si(Me)_3$	$C_{18}H_{37}(CH_2CH_2O)_{10}OH$; no structure post-grafting	Sensor, capacitive devices ⁵⁸
34) Dimethyldiethoxysilane $H_3C-Si(OEt)_2-CH_3$	TEOS, CTAB; 2D hex post-grafting	Low- k dielectric materials ¹⁴⁷

Table 1 Functional organosilanes and properties of resultant thin film mesophases (*Continued*)

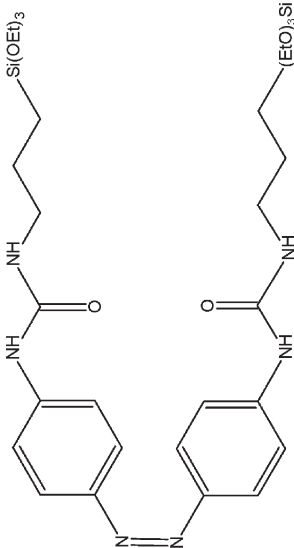
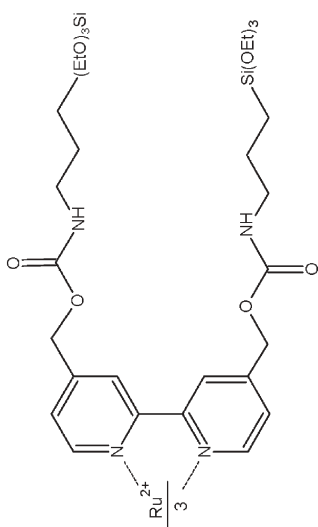
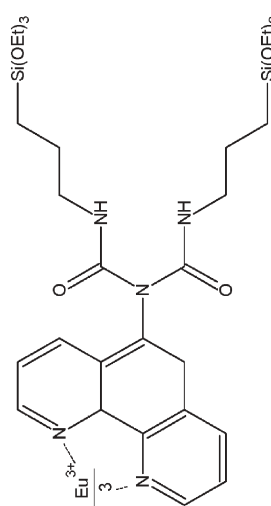
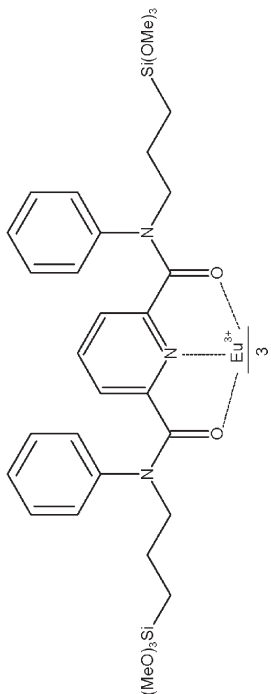
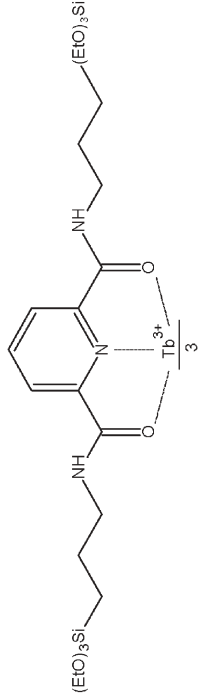
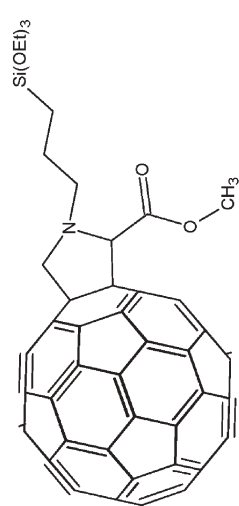
Functional organosilanes	Experimental conditions and results	Properties/applications and references
<p>35) 4,4'-Bis(3-triethoxysilylpropylureido)azobenzene</p> 	Self-assembl; lamellar	Optomechanical actuation ¹⁰³
<p>36) Ru(II) 4,4'-hydroxymethyl-2,2'-bipyridine (derivatized with isocyanatopropyltriethoxysilane)</p> 	TEOS, CTAB; 2D hex	106,108
<p>37) Silanized Eu(III) phenanthroline</p> 	TEOS 2D hex	Nonlinear optical materials, tunable solid-state lasers ¹¹⁰

Table 1 Functional organosilanes and properties of resultant thin film mesophases (*Continued*)

Functional organosilanes	Experimental conditions and results	Properties/applications and references
<p>38) Eu(III) bis(<i>N,N'</i>-phenyl-3-trimethoxysilylpropyl)-2,6-pyridine dicarboxamide</p> 	TEOS, CTAB; 2D hex	106,127
<p>39) Tb(III) <i>N,N'</i>-bis(3-triethoxysilylpropyl)-2,6-pyridine dicarboxamide</p> 	TEOS, CTAB; 2D hex	106,127
<p>40) <i>N</i>-[(3-Triethoxysilyl)propyl]-2-carbomethoxyfulleropyrrolidine</p> 	TEOS, F127/Brij 58; poorly organised structure	Optically encoded information storage for read only materials (ROMs) ¹⁰²

hydrolysis time. To overcome these problems, a pre-hydrolysis step of the organosilane in a weak acidic medium⁹⁷ and/or the use of a cosolvent are required. The choice of cosolvents is limited; the cosolvent must not only dissolve the desired organofunctional molecule but also be miscible with the starting sol without causing organosilane gelation and without affecting either the film optical quality or the mesostructured long range order. Moreover, the cosolvent must present an evaporation ability close to that of ethanol and assure a good wettability towards coating substrates. The cosolvent most commonly employed in the literature is tetrahydrofuran. This cosolvent, used in place of ethanol or in a mixture with ethanol, has been successfully employed for preparing well-organised thin films with monomers,^{57,100,101} β -diketones,⁶⁰ C_{60} derivatives,¹⁰² bridged silsesquioxane¹⁰³ or with MTEOS-based matrices.¹⁰⁴

The functionalisation of probes containing a basic function, typically an amino group, presents another difficulty. Acidic conditions in EISA are important to make films which present good (optical) quality, which is a very important feature for applications in optics and optical sensors. The basic function catalyses hydrolysis and condensation reactions of the silica precursor in the presence of water and can yield the fast gelation of the sol. In order to prevent these two phenomena, amino groups can be first neutralised with a strong acid prior to the addition of the silica precursor.^{98,105} A subsequent treatment of the films with ammonia allows the recovery of the amino group through deprotonation of the ammonium.⁹⁸ However, in the particular case of metal complex incorporation, a too high loading could also lead to a gelation process as was observed for a ruthenium complex which catalysed the condensation of silica species.¹⁰⁶

3.1.3 Chemical reactions in the organic domain. The incorporation of polymers into nanostructured films can lead to specific difficulties as pointed out by Smarsly *et al.*¹⁰¹

- In general, polymers undergo substantial changes in their hydrophobic/hydrophilic behavior compared to monomers, which may eventually lead to phase separation after polymerisation and can cause modifications or damages to the mesostructure. Indeed, since the polymerisation, especially of acrylates, can be strongly exothermic, the mesostructural order can become significantly damaged due to the fragility of the silica network at this stage and the temperature dependence of self-assembly.

- In a classical free-radical polymerisation, the degree of polymerisation and the amount of cross-linking strongly depend on various parameters such as the nature of the initiator and its concentration, *etc.* The optimum synthesis conditions for thin films may be different from those required for bulk systems.

- Because organosilanes containing both an alkoxy group and a double bond can be used as a link between the polymer and the inorganic matrix, significant reactivity of the molecule's double bond is essential. If the reactivity is too high, however, the coupling agent may already react before dip-coating or spin-coating, hence impairing the EISA process. Also, too high reactivity might lead to a distortion of the mesostructure during the polymerisation. Therefore, optimum

conditions have to be found, balancing the favorable and damaging properties of the coupling agent. For example, it has been shown that the quality of lamellar nanocomposites resulting from the polymerisation of methacrylate species incorporated *via* a one-pot process in mesostructured thin films depends on the coupling agent linking the polymeric phase and the silica framework.¹⁰¹ While trimethoxy(7-octen-1-yl)silane showed low reactivity of the double bond, the polymer/silica films were of reasonable quality with respect to the quality of ordered mesostructure and the swelling property of the polymers. In contrast, coupling agents such as 3-(trimethoxysilyl)propyl acrylate or 3-(trimethoxysilyl)propyl methacrylate containing more reactive acrylate double bonds massively distorted the film mesostructure, yielding less ordered mesophases.

3.1.4 Spectroscopic investigations of probe localisation in hybrid mesostructured thin films. Most of the studies dealing with the localisation of probes (*i.e.* organic functionality grafted to silica) in mesostructured thin films and the influence of incorporated probes on mesostructuration concern the CTAB/TEOS system. In order to control the final properties of functional thin films, it is of great importance to localise perfectly the probes in the mesostructure. With regards to mesostructured thin films made with ionic surfactants such as CTAB, the structure can be divided into 3 main regions:^{106–108} the silica framework (Fig. 5a, zone I), the organic region composed by the hydrophobic core of the micelles (Fig. 5a, zone II), and the ionic interface formed by the charged surfactant heads, the hydrosilylated silica surface (Fig. 5a, zone III).

This organic/inorganic phase separation is also obtained with non-ionic surfactants such as triblock copolymers (*i.e.* poly(ethylene oxide)–poly(propylene oxide)–poly(ethylene oxide) PEO–PPO–PEO)-based thin films (Fig. 5b). However,

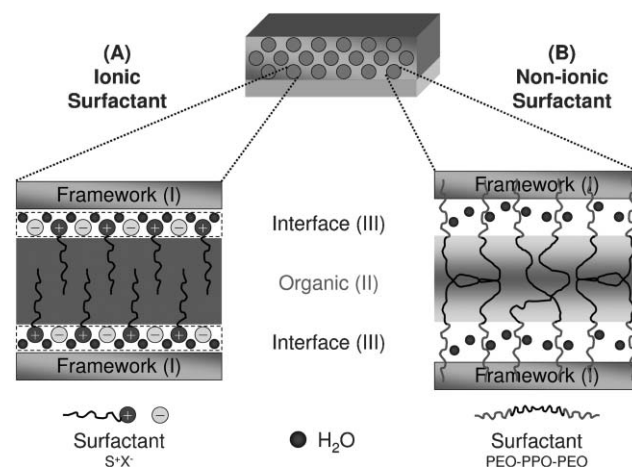


Fig. 5 Sketch of the three main regions of mesostructured sol-gel films. In the case of ionic surfactants (CTAB—left side), the framework (I) consists of silica or modified silica, the organic region (II) containing the hydrocarbon tails of the surfactant templates, and the ionic region (III) containing the surfactant headgroups, the counterions, and residual solvent. For non-ionic surfactants (triblock copolymers—right side), the interface (III) is formed by poly(ethylene oxide) groups and water. Adapted from references 106,107,109.

in this case, the limits between the three phases, silica wall, hydrophobic PPO block and hydrophilic PEO block, are less defined mainly because of interpenetration of the PEO and silica networks.¹⁰⁹

According to the literature, the silylated functions can be classified into two categories:

- Monosilylated compounds, $F-S-Si(OR)_3$, constituting the most common category studied (with $-OR$ condensable groups, F the functionality and S the spacing group).

- Multisilylated probes of general formula: $F(S-Si(OR)_3)_n$, mainly composed by $(OR)_3Si-F-Si(OR)_3$ bridged silsesquioxanes and rare earth complexes with silylated organic ligands.

The localisation of probes inside the mesophase has been investigated either directly by spectroscopic techniques such as fluorescence,^{106–108,110} UV-visible absorption⁶⁰ and micro-Raman⁹⁹ spectroscopies and/or indirectly by studying structural changes induced by the incorporation of probes (*e.g.* variation of the lattice parameters,^{98,99} phase transition,^{60,98,99} formation of mesophase at very low surfactant/TEOS ratio⁹⁷).

The localisation of the probe is governed by its physico-chemical properties. Several factors have to be taken into account such as the hydrophilic/hydrophobic balance of the probe's molecule, the number of anchoring functions ($-OR$)₃, the length and the nature of the spacing group (group S between the functionality F and the anchoring function $-Si(OR)_3$), the nature of the functionality F (hydrophobic, hydrophilic, ionic, polar, apolar, aromatic for example).

A general trend is commonly observed with probes presenting multiple trialkoxysilane functionalities. They are localised inside the inorganic network, as was observed with multisilylated rare earth complexes,^{106–108,110} or even compose the walls of the framework as observed with hybrid bridged silsesquioxanes.^{31,111,112} The emission properties of such rare earth complexes in mesostructured films give evidence of the location of this ion in the mesophase. The similarities in the emission spectra and lifetime values observed for amorphous (films synthesised without surfactant) and mesostructured films suggest that the rare earth ions lie in a similar environment in the two types of films. Their emission characteristics are, in both cases, typical of organic complexes covalently anchored to a sol-gel silica matrix. In the particular case of Eu^{3+} , the ratios of the $^5D_0 \rightarrow ^7F_2$ and $^5D_0 \rightarrow ^7F_1$ transition intensities, which are sensitive to the symmetry around the ions, remain identical in both the mesostructured and the amorphous films.¹⁰⁶ The monoexponential decays recorded in all cases for europium are indicative of a single average site distribution for each ion. In the case of multisilylated rare earth complexes, the presence of multiple $Si(OEt)_3$ functional groups results in the chemical bonding of the luminescent centers within the silica framework. Hybrid bridged silsesquioxanes,^{31,111,112} but also the monosilylated methyltriethoxysilane,^{96,104} have been successfully used as precursors instead of TEOS leading to mesostructured thin films with added properties (hydrophobicity, low dielectric constant). Concentrations as high as 100% in organosilane have been reached.

However, most of the common probes are monosilylated with a general formula $F-S-Si(OR)_3$. Such molecules possess two different groups, one carrying the functionality and the

other being the condensable groups. Both groups simultaneously interact with two different regions of the mesostructure. The condensable $-OR$ groups allow the formation of chemical bonds between the molecule and the framework. It is interesting to point out at this stage that even if most studies reported in the literature concern pure silica frameworks, the use of such probes is also compatible with organosilica frameworks (bridged bistrialkoxysilanes¹¹²); or surprisingly, with transition metal oxides like ZrO_2 or TiO_2 .¹¹³ The localisation of the functionality F is mainly governed by the “philicity” concept (or “like” dissolves “like”) but also by specific interactions such as cation- π ¹¹⁴ or ionic.¹⁰⁶

The philicity concept exploits the physical affinities of the active ingredients for a particular environment (for example, the affinity of a lipophilic dye for the core of surfactant micelles) to predict the distribution of the molecule in a specific region. A general trend observed is the solubilisation of lipophilic molecules in the hydrophobic micelle core and the placement of hydrophilic molecules either in the ionic interface or in the framework. Since micelle formation is the important step of mesostructured film elaboration, hydrophobic molecules will be incorporated into the film at this early stage of the structuration process. At the critical micelle concentration (cmc), the individual surfactant molecules aggregate to form micelles and the lipophilic dopant molecule is incorporated therein. The incorporation of a silylated β -diketone in thin films was recently investigated.⁶⁰ These are compounds that exist mainly in two tautomeric forms in equilibrium. As the keto-enol equilibrium is extremely solvent-sensitive, a spectroscopic study allowed the localisation of the silylated probes in thin films. Indeed, the absorption spectra of the β -diketone in thin films, whatever the mesophase, have the same aspect that of the probe dissolved in THF, indicating that the β -diketone environment is apolar, suggesting their localisation inside the hydrophobic core of the micelles.

Zink *et al.*^{106,107} observed that the localisation of a silylated positively charged ruthenium complex depends on the surfactant charge. In SDS (anionic surfactant) based thin films, the ionic complex resides in the ionic region at the interface between the organic and inorganic regions, while, in mesostructured thin films made with cationic surfactant (*i.e.* CTAB), the complex is located in the silica network. The emission maximum ($\lambda_{max} = 665\text{--}669\text{ nm}$) of the complex is identical in amorphous films and in CTAB-mesostructured thin films¹⁰⁶ while the same blue shift ($\lambda_{max} = 650\text{ nm}$) is observed in SDS mesoporous thin films and in methanol.¹⁰⁷ These spectroscopic results suggest that the electrostatic repulsion between the positively charged Ru complex and cationic CTAB headgroups makes the ionic region less hospitable than the silicate matrix, thus forcing the Ru complex to enter into the silicate matrix.

Cagnol *et al.*⁹⁸ observed that the structure of the final mesophase depended on the loading rate of (2-phenylethyl)-trimethoxysilane in thin films. For low amounts of probe, the mesostructure was not influenced by the presence of the organosilane, presenting a cubic structure ($Pm\bar{3}n$), whereas for high amounts of probe, a 2D-hexagonal ($p6m$) phase was formed. Such phase transitions are commonly observed when the $[CTAB]/[SiO_2]$ ratio increases,⁶⁷ inducing a decrease in the

curvature of the micelles. It is generally agreed that two kinds of sites are available when a molecule is solubilised inside micelles: one near the polar head and the other between alkyl chains in the hydrophobic core of the micelles.^{115,116} It has been shown¹¹⁷ that the first site occupied by aromatic compounds is near the polar head of CTAB surfactants due to specific interaction between the π system and the quaternary ammonium.^{114,118,119} Once the first sites are saturated, the solubilisation occurs in the hydrophobic part of the micelles, inducing a decrease of the curvature of the micelles and causing a phase transition.

The length and the nature of the spacing group, S, could hinder the natural placement of hydrophobic functionality inside the micelles. For instance, with the same functionality (*i.e.* phenyl group) and the same relative amount of probes, no variation of mesophases was observed with the phenyltriethoxysilane, in contrast to (2-phenylethyl)trimethoxysilane.⁹⁸ This result could be explained by a physical impossibility of the aromatic functionality to fully reach the hydrophobic part of the micelles in the case of the phenylethyl-based precursor, thus “preventing” the swelling of the micelles and the decrease of the interface curvature. This geometrical criterion is in balance with all other parameters described previously. Consequently, the role of the organic function during the self-assembly is complex, mainly because the key parameter leading to a particular mesophase is not always predictable. The functionality and the spacing group may interact more or less strongly with the silica wall, with the surfactant head group, and with its hydrocarbon tail, affecting or not the curvature of the hybrid interface.

3.1.5 Effects of probes on mesostructuration: phase transitions and variations of the lattice parameters. We have seen previously that spectroscopic techniques (*i.e.* absorption, UV-visible or fluorescence spectroscopies) are a useful tool to localise the silylated probes inside mesostructured thin films. However, the incorporation of probes inside thin films could also cause structural changes, from variations of the lattice parameters to phase transitions and even the formation of a mesophase for a (very low) surfactant/silica molar ratio leading to an amorphous thin film without silylated probes. All these changes give an indirect localisation of the organosilane inside mesoporous thin films.

The changes of the lattice parameters with an increasing amount of organosilane could be an indication of its preferential localisation at the ionic interface, near polar heads of the micelles.^{98,99} In the system CTAB–TEOS, the incorporation of a positively charged organosilane, 2-(trimethoxysilyl)ethylpyridinium, induced the formation of a 2D-hexagonal phase (*p6m*), regardless of the loading ratio.⁹⁸ The authors observed a progressive increase of the interreticular distances $d(01)$ with increasing incorporated protonated ammonium organic functions. This observation also occurred with the two other positively charged groups studied (*i.e.* 3-(2,4-dinitrophenylamino)propyltriethoxysilane and 3-aminopropyltriethoxysilane). These results could be primarily attributed to the cationic character of the incorporated functions. Usually, in acidic conditions, the bromide is intercalated between the ammonium head group and the silica wall through electrostatic interactions ($I^+X^-S^+$).⁷³ In this case, the electrostatic repulsion between the two positively charged groups (*i.e.* the polar head of the surfactant and the functionality, F, of the organosilane) governs the formation of the mesophase with a main localisation of the probe in the ionic interface, even if a swelling effect could be involved. The results are in agreement with the spectroscopic study of the group of Zink concerning the localisation of a positively charged silylated ruthenium complex in CTAB-based mesoporous silica thin films.¹⁰⁶

The incorporation of probes could also lead progressively to a destructuration of the mesophase with few changes in the lattice parameters, as in the case of 3-cyanopropyltriethoxysilane from a well ordered 2D-hexagonal structure to a vermicular phase.⁹⁹ This modification could be explained by a solubilisation of the cyanopropyl groups inside the surfactant micelles. Another example of phase transition was reported with the incorporation of a silylated β -diketone compound.⁶⁰ The addition of increasing amounts of triethoxydibenzoylmethane for a fixed CTAB/silica molar ratio induces mesostructural evolution in thin films. The following sequence was observed: cubic phase (*Pm3n*) < mixture of cubic (*Pm3n*) and 2D-hexagonal (*p6m*) < pure 2D-hexagonal phase < lamellar phase (Fig. 6). Such phase transitions are explained in terms of variation in the packing parameter g ($g = V/a_0l$, where V is the total volume of the surfactant chain, a_0 is the effective head group area and l is the surfactant chain

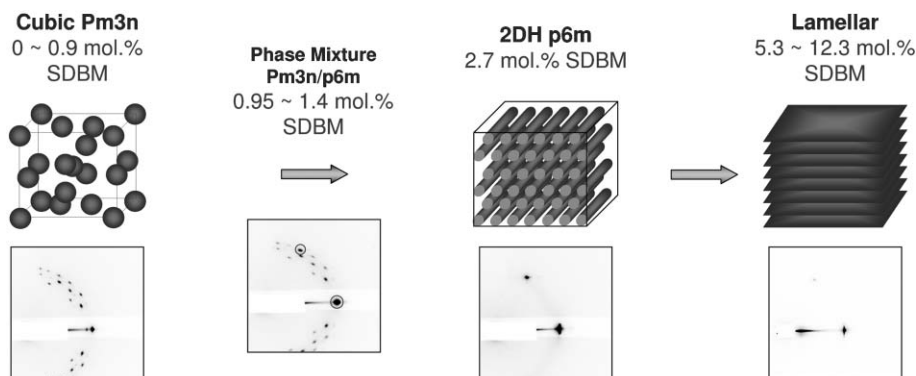


Fig. 6 Phase transitions observed in thin films with addition of increasing amounts of triethoxydibenzoylmethane for a CTAB/silica molar ratio fixed at 0.14. Adapted from reference 60.

length), which is related to the modification of the interfacial curvature.¹²⁰ For silica systems, it has been shown that an increase of g (*i.e.*, a decrease in the curvature of the micellar motif) leads to phase transitions along the sequence micellar cubic ($Pm3n$) \rightarrow hexagonal ($p6m$) \rightarrow lamellar.^{67,121} Therefore, the increase of the packing parameter can be due to solubilisation of large species (triethoxydibenzoylmethane) preferentially in the hydrophobic part of micelles during evaporation of solvents, leading to an increase of the total volume associated with the surfactant chain, V . This mechanism is supported by UV-visible experiments performed on hybrid thin films.⁶⁰ In this case, the incorporation of large species causes direct phase transitions without modifications of the lattice parameters.

This co-solvent effect allows the formation of a mesophase for conditions at which mesostructured thin films are not usually obtained (*i.e.* very low surfactant/silica ratio). The synthesis of mesoporous thin films with 10% mol of perfluoroalkylsilanes with long chains, typically tridecafluoro-1,1,2,2-tetrahydrooctyltriethoxysilane and heptadecafluoro-1,1,2,2-tetrahydrodecyltrimethoxysilane, have been achieved⁹⁷ with a sol containing a ratio CTACl/Si \sim 0.004. It is interesting to point out, following the phase diagram of the CTAB/Si/H₂O ternary system,⁶⁷ that the lowest CTAB/Si ratio leading to the formation of mesostructured thin films is equal to 0.10. Moreover for this last ratio, we could expect only a 3D-hexagonal mesophase ($P6_3mmc$), which is a structure with a higher curvature of the micellar interface than the 2D-hexagonal phase ($p6m$) observed with the addition of the perfluoroalkylsilanes. This result suggested that perfluoroalkylsilanes also act as a structure-directing agent when the reactant is mixed with a small amount of surfactant. Indeed, hydrolysed perfluoroalkylsilanes carrying hydrophilic silanol head groups and long hydrophobic perfluoroalkyl chains are clearly amphiphilic molecules.

We have seen that the function, F , could develop direct interactions with surfactant-head groups. These interactions increase the area of the surfactant's head group, promoting higher curvature of the micelles promoting the $Pm3n$ structure. The opposite effect on the curvature would be obtained by increasing the volume of the hydrophobic micelle core (swelling effect). However, in a particular system, one has to keep in mind that the effect of each function is more subtle and cannot be sketched by only these two extreme effects.

3.1.6 Properties of thin films and potential applications. Even though some studies have dealt with potential applications concerning absorption of polluting species such as organophosphorus compounds,^{112,122} grafting sites (typically $-NH_2$ or $-COOH$ groups) for binding biomolecules such as enzymes, antibodies and other proteins^{105,123} or creating synthetic ion channel devices,^{105,123} the majority of research is dedicated to the study of applications in the field of optical sensors,^{53,59,60,124} low- k dielectrics,^{31,58,96,97,111,104,125} photonic devices^{102,126,127} and environmentally responsive materials (molecular valves or gates^{63,64} or controlled release/membranes with switchable permeabilities¹²⁸) which can be obtained *via* rapid-prototyping procedures.^{53,124}

3.1.6.1 Optical sensors. Hybrid sol-gel glasses are commonly used as supports in the development of optical sensor devices because they are transparent, chemically inert, thermally and mechanically robust, photostable, easily processed and they allow the embedding/grafting of molecular probes.¹⁴ However, the poorly ordered microporosity of such materials is sometimes a limiting factor to the homogeneous and fast diffusion of analytes inside the sensing matrix. On the other hand, mesostructured mesoporous thin films with their larger open porosity and their high surface area should improve analyte diffusion and accessibility towards supported probes. Moreover, both their monomodal narrow pore size distribution and their controlled porous connectivity make them much more resistant to the huge capillary stresses usually responsible for the instability and the collapsing of mesoporous xerogels in liquid work conditions (*i.e.* successive solvent dipping and drying sensing cycles). The choice of the mesophase (2D or 3D geometry) could be adjusted to specific properties of the sensor (*i.e.* diffusion, accessibility, mechanical stability). In addition to that, the leaching of the functionality which is one of the greatest problems in hybrid sensor applications, is prevented by the anchorage of the sensing probe to/within the framework.

Simultaneously reported by two research groups,^{53,59,124} the simplest optical sensor application developed are pH sensors based on covalently linked fluorescein derivatives, a pH-sensitive dye. Wirnsberger *et al.*⁵⁹ synthesised a sensor by reacting fluorescein isothiocyanate with 3-aminopropyltriethoxysilane and adding it to a F127 block copolymer film preparation. This functionalisation ensures that the dye is covalently anchored onto (or within) the SiO₂ wall during mesostructure synthesis. After dip-coating, the \sim 900 nm thick films were dried for approximately 10 days at room temperature and finally stabilised at 70 °C for 3–5 days. This prolonged drying treatment is necessary in order to achieve a sufficiently high silica condensation in films before block copolymer extraction by ethanol at 80 °C.

These sensors operated by recording the emission of the anchored fluorescein dye. Similarly to what was observed for fluorescein in solution, the integrated emission increased with increasing pH. The thin film sensors acted analogously to the dye in solution, except that the pK_a value was shifted from 6.4 in solution to \sim 7.3 in the thin films. The broadening of the titration curve observed for the mesoporous film was attributed to two factors. The first one involved an inhomogeneous dye environment and the second one was related to the difficulties, encountered even in solution, of distinguishing the three pK_a of fluorescein ($pK_{a,1} = 2.08$, $pK_{a,2} = 4.31$, $pK_{a,3} = 6.43$). The response time of the mesoporous hybrid thin films is on the order of \sim 7 s for a 95% change in the emission intensity. This response time is much shorter than the value measured in sol-gel glasses.^{129–131} The fast response time was attributed to the high porosity of the dye-carrying mesoporous thin film, since the open pores enable a fast diffusion of the solution toward the dye molecules.

Brinker and co-workers used a more elaborate approach involving microfluidics, to produce a similar pH sensor.^{53,124} They first patterned amine-modified cubic mesoporous silica using selective de-wetting of patterned surfaces made by

surface assembled monolayers, SAMs (for more detailed information, see section 3.1.6.6). The pattern consisted of three L-shaped patterns with a viewing cell, created by interdigitating long narrow lines with large pads on the ends used to load solutions (Fig. 7). The sol was prepared by adding aminopropyltrimethoxysilane to a TEOS/Brij-56 sol. Selective de-wetting during dip-coating (1) followed by calcination results in a patterned, amine-functionalised, cubic mesoporous film as is evident from the plan-view TEM micrograph (inset A). The moderate calcination allowed the removal of the surfactant while maintaining the amine functionality, as confirmed by NMR. The dye conjugation reaction (2) was realised by immersion in a solution of 5,6-FAM SE (5,6-carboxyfluorescein, succinimidyl ester), prepared in dimethylsulfoxide (DMSO) followed by exhaustive, successive washing in DMSO, ethanol, and water to remove unreacted dye. Finally, solutions of different pH were placed on the pads and transported to the cell by capillary flow. Comparison with solution fluorescence spectra indicated that dye molecules covalently attached to the mesoporous framework retain similar features to those in solution. This application clearly demonstrates that these highly ordered mesoporous transparent thin films with high mechanical robustness are well-suited materials for fast response optical sensors. Future applications in this area also might use patterning methods such as ink-jet and micro-pen printing of mesostructures in order to generate optical multi-sensor arrays (section 3.1.6.6).

Mesoporous thin films functionalised with triethoxysilyl-dibenzoylmethane (SDBM) exhibiting a high selectivity and sensitivity to metal cation pollutants such as uranyl were developed by the Paris group.⁶⁰ After surfactant extraction, the spectral responses of functionalised thin films with [SDBM]/[Si] ratios of 2.7 and 5.3% (with *p6m* and lamellar phases respectively) were studied in aqueous solutions with various metallic cation salts: Cd(II), Ce(III), Co(II), Cr(III),

Eu(III), Ni(II), U(VI), Cu(II) and Fe(III). For a demonstration of their application as chemical sensors, films were soaked in the cation aqueous solutions under gentle stirring for 30 seconds, then washed with ethanol and dried. The *in situ* monitoring during these first 30 seconds shows that optical changes occur for three cations only (Cu(II), Fe(III) and U(VI)) in the UV domain and the formation of colored complexes for the two last cations only (orange with Fe(III) and yellow for U(VI)) (Fig. 8). The selectivity of films towards Cu(II), Fe(III) and U(VI) cations was explained by a shorter complexation equilibrium time compared to other metallic cations. According to Stary and Hladky,¹³² even if the dibenzoylmethane (precursor of the SDBM) compound allows the extraction of many metals in solution, the extraction equilibrium time depends on the metallic cations (from a few minutes to several days). The selectivity observed with thin films is thus due to the short time of experiments (30 seconds) and not due to the intrinsic selectivity of the SDBM molecular probe.

The immersion induces the emergence of a new absorption band in the visible region. The absorption spectrum after complexation is assigned to the superposition of SDBM, uranyl and the SDBM-U(VI) colored complex spectra. Therefore, a near-visible sensing range was selected for uranyl cation detection which is optimal at 400 nm. Complexation kinetics were observed to be dependent upon the concentration of U(VI), ranging from seconds at high concentrations (above 100 ppm) to minutes at low concentrations (below 100 ppm). The uranyl detection limit is attained for a 1 ppm solution, which is excellent for such a simple absorbance variation sensing method.

Classical amorphous sol-gel functionalised thin films synthesised without surfactant showed similar UV-visible spectra but did not show efficient detection of any tested metallic cations. Finally, the reversibility and reproducibility

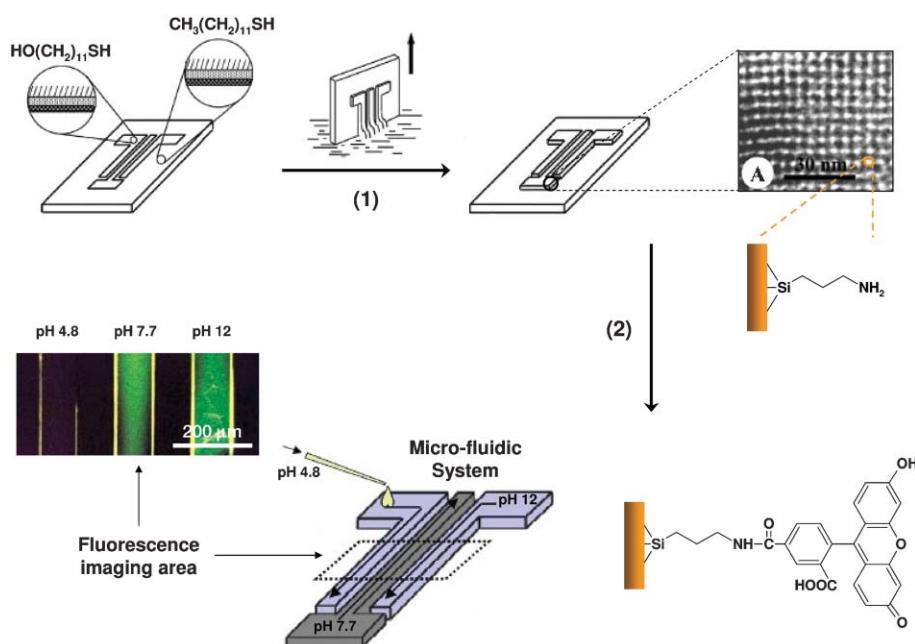


Fig. 7 Patterned pH-sensitive mesostructure formed by selective de-wetting. Adapted from references 53,124.

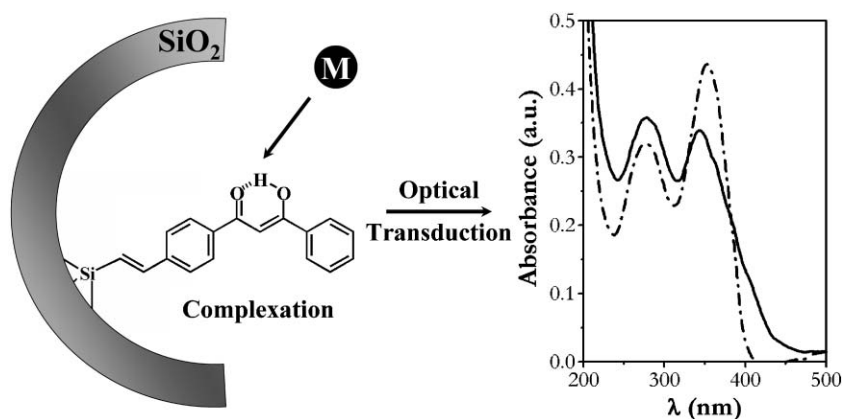


Fig. 8 Evolution of thin film responses with a 2D-hexagonal mesostructure containing a [SDBM]/[Si] ratio of 2.7% upon immersion in a 100 ppm uranyl nitrate solution. Adapted from reference 60.

of films, which are crucial parameters, were tested using repeated detection regeneration cycles. A simple treatment in solution with acetylacetone permits regeneration of the films with good preservation of their sensing properties, even after several complexation–regeneration cycles. For a 2D-hexagonal phase reproducibility was between $\pm 3\%$ and, more surprisingly, between $\pm 7\%$ for the lamellar structure. The stability of such a hybrid lamellar phase *versus* washing–complexation–regeneration cycles could be explained by the presence of π -stacking interactions between SDBM compounds located on the opposite sides of the silica layers.

It is interesting to point out that following the working conditions of such silica-based sensors, *i.e.* basic media, a partial degradation of the matrix could occur. Recently, Soler-Illia *et al.*¹¹³ reported the synthesis of highly ordered hybrid mesoporous bifunctional thin films from a mixture of TiCl_4 or ZrCl_4 and organosilanes $\text{R-Si}(\text{OEt})_4$ (R = amine, phenyl and thiol groups). Such metal oxide matrices, especially with zirconia, are particularly interesting because of the higher chemical stability of the oxides than silica.

3.1.6.2 Low- k dielectric properties of mesostructured hybrid films. Dielectric materials with a low dielectric constant k are currently in demand for future integrated circuits. By extension of the pristinely-used isolating layers of microelectronics, SiO_2 ($k \sim 3.8$) is one of the materials investigated in this direction. However, as devices are becoming smaller, lower dielectric constants are required ($k \leq 2$). One of the most promising applications of these mesoscopically-ordered silica films is their use as insulators in integrated circuit devices due to their low dielectric constant.⁶⁵ Indeed, the strategies to lower the dielectric constant are limited. Usually two issues are targeted: (i) increase the porosity and (ii) decrease the molecular polarisability of the matrix (for a better understanding of low dielectrics see the excellent review in ref. 133). However the effect of the global density (number of molecules per unit of volume, which determines porosity of films and density of the wall) on the dielectric constant film is stronger than the effect of molecular polarisability, since reducing the density allows the reduction of the dielectric constant to the extreme value close to unity (corresponding to the dielectric

constant of dry air). It is thus obvious that mesostructured thin films, with their large porosity, are promising candidates as low k materials. Amorphous silica films, used in microelectronics, have a density of $2.1\text{--}2.3\text{ g cm}^{-3}$ and a refractive index of 1.46. The high frequency dispersion of dielectric constants ($k \sim 4$ in the low frequency region and $k \sim 2.15$ in the range of visible light) is related to the high polarisability of the Si–O bonds (distortion polarisation). Lowering the k value can be accomplished by replacing the Si–O bond with a less polarisable bond such as Si–R. This approach consists of doping the silicate glasses with carbon and/or fluorine by introducing alkyl or fluoroalkyl groups in the matrix. Moreover, both fluorine and carbon increase the interatomic distances or “free volume” of silica, which provides an additional decrease of dielectric constant. In addition to that, the introduction of such organic groups in the matrix provides a hydrophobic environment which limits the parasite adsorption of highly polarisable water molecules in pores. Therefore the different approaches involve the modification of either the nature of the walls (*i.e.* bridged polysilsesquioxanes^{31,111} or methyltriethoxysilane^{96,104}), or the pore surfaces with one-pot synthesis functionalisation of perfluoroalkoxysilanes⁹⁷ or trimethylchlorosilane.¹²⁵ A post treatment with hexamethyldisilazane could improve the hydrophobicity of thin films by reacting with silanols.^{58,125} Finally, a compromise must be found between porous volume, mechanical stability, hydrophobicity and dielectric constant.⁹⁶ The efficiency of this approach in promoting low dielectric constant thin layers has been claimed many times. However, the effective dielectric constants are not usually measured.

3.1.6.3 Photonic applications of mesostructured hybrid thin films. Most of the described examples of mesostructured hybrid films using luminescent molecules were designed to probe the film formation,^{134–137} to elaborate waveguides or laser arrays⁶² or to study the energy transfer between two organic dyes located in the micelles.¹³⁸ However, the localisation of the probes in the micellar part of thin films could limit their potential applications mainly due to leaching of the dye.

In 1999 Lebeau *et al.*¹²⁶ reported for the first time the “one-pot” synthesis of functionalised mesoporous silica thin films

with a silylated dye, 3-(2,4-dinitrophenylamino)propyl-triethoxysilane. 2D-Hexagonal thin films were obtained by direct chemical synthesis involving the co-condensation of tetraethoxysilane and 3-(2,4-dinitrophenylamino)propyl-triethoxysilane in the presence of the surfactant, hexadecyltrimethylammonium bromide. Optical properties of the dye-functionalised surfactant-extracted mesoporous materials were investigated by UV-vis and fluorescence spectroscopies. They observed that the optical activity of the dye moiety was retained when it was covalently linked to the silica network of the mesostructure. They demonstrated that ordered organo-silica thin films with a high dye loading (typically 10 mol% 0.9 TEOS : 0.1 dye) can be prepared by the one-pot synthesis, to produce transparent thin films with optical properties and mesoscale architecture.

The well-organised local separation of organic/inorganic regions in mesostructured composites provides substantial versatility for adjusting host/guest optical properties. The hydrophobic regions are compatible environments for organic dopants, enhancing their overall solubilities and preventing their aggregation. In addition, the rigid inorganic framework protects and stabilizes the included species but could also incorporate other functionalities.

As previously described in section 3.1.4, the localisation of probes inside the three main regions constituting mesostructured materials can be controlled by several factors. It has been shown that philicity and the number of trialkoxysilane groups per dopant molecule could affect the placement of the probes in mesostructured thin films. In the context of nanostructured hybrid thin films, philicity operates by placing hydrophobic organic molecules inside the surfactant micelles. However, with lanthanide complexes, the presence of ligands containing two trialkoxysilane groups (up to six trialkoxysilyl groups per metal complex) leads to the localisation of the rare earth complex in the silicate framework by co-condensation of silicate precursor (TEOS for example) with the trialkoxysilyl groups surrounding the metal.

Zink's group¹²⁷ used this preferential placement of probes to study the energy transfer between two luminescent dyes located in two different spatially-separated regions: the rhodamine R6G incorporated in the micelles of CTAB and Eu^{3+} and Tb^{3+} complexes chelated by alkoxysilylated ligands.

The films consist of a silicate framework that holds in place a two-dimensional hexagonal structure with a lattice spacing of 40 Å templated by an ionic surfactant (CTAB). Pairs of molecules consisting of an energy donor lanthanide complex and an energy acceptor rhodamine dye (R6G) are placed in the framework and the surfactant, respectively, as was confirmed by fluorescence spectroscopy. It is interesting to point out that for films obtained at an R6G : CTAB mole ratio of 15 : 1000 in the precursor sol, the fluorescence peak of the mesostructured film is 27 times more intense than that of the amorphous film, and the excitation peak intensity of the mesostructured film is 42 times more intense than the excitation peak of the amorphous film. The higher fluorescence intensity of R6G in nanostructured films relative to amorphous films shows that the presence of CTAB affects R6G luminescence. It was also noted that the fluorescence intensity obtained from nanostructured films containing R6G increased with increasing

R6G concentration, reached a maximum at R6G : CTAB = 24 : 1000, and then decreased as the R6G concentration increased further due to concentration quenching.

Quantitative measurements of energy transfer between Tb^{3+} and R6G in the mesostructured films were made and used to calculate the distance between the donor and acceptor. Steady-state fluorescence and photoexcitation spectra and the R6G and Tb^{3+} complex's luminescence lifetimes showed that excited Tb^{3+} complexes transfer their energy to R6G molecules in a concentration-dependent manner. The excitation spectra showed that absorption of light by the lanthanide complex resulted in emission of light from the R6G. The lifetime of the lanthanide complex decreased, and that of the R6G increased. Quantification of the data according to Förster theory showed that the separation between Tb^{3+} and R6G can be large enough at low concentrations to reach the limit where nearly no quenching occurs (~ 65 Å) but that it gets no smaller than ~ 29 Å at high R6G concentrations.

The interest in hybrid matrices for preserving the optical properties of a molecule was also shown with molecules known to exhibit strong reverse saturable absorption (RSA). The excited-state absorption of such dye molecules is stronger in some spectral ranges than the ground-state absorption. As a consequence, such chromophores become less transparent as the incident intensity increases. Such a property can be used to create optical limiters, which transmit light at low powers and become opaque for increasing light inputs. Efficient solid-state reverse saturable absorbers were made by entrapment of phthalocyanines and fullerene C_{60} in hybrid matrices.^{139–142} However, the low solubility of fullerene C_{60} or its derivatives in water leads to aggregation, which causes a decrease of RSA. Improved optical-limiting performances were obtained by the use of grafting of C_{60} to the matrix backbone. Fullerene C_{60} derivatives have been functionalised with trialkoxysilane groups to increase their concentration in the final matrix with no clustering effects.^{141–145} Recently, the synthesis of functionalised mesostructured thin films with silylated C_{60} derivatives has been reported.¹⁰² Three fullerene derivatives have been employed with amphiphilic block copolymers both as structure directing agents and doping molecules in one-pot synthesis of self-assembled 2D-hexagonal and cubic porous silica mesostructures through an evaporation-induced self-assembling procedure. Calcination of the samples at 280 °C almost completely removed the block copolymer from the silica matrix without substantial loss of the fullerene additive. The authors observed a homogeneous dispersion of the fullerene within the pores. Upon irradiation with laser light at 632.8 nm, the fullerene-doped mesostructured materials exhibited photoluminescence at room temperature, which was not observed in the amorphous silica matrix. According to the authors,¹⁰² the fullerenes “confined” in the micelles hydrophobic core will be the source of the photoluminescence quantum confinement effect. This property could open the route to potential applications in optically encoded information storage for read only memory materials (ROMs).

3.1.6.4 Molecular valves or gates. To expand the range of accessible properties, various organic functional groups have been covalently incorporated onto the pore surfaces of

mesoporous materials (Table 1). However, these modifications have provided mainly “passive” functionality, such as controlled wetting properties, reduced dielectric constants, or enhanced adsorption of metal ions. By comparison, materials with “active” functionality would enable properties to be dynamically controlled by external stimuli, such as pH,¹²⁸ temperature,^{63,64,128} or light.^{63,64} Materials that predictably respond to pH, temperature, light, biomolecules, or electric fields are of potential interest for applications in microfluidics, microvalves, controlled drug release, sensors, optical switches, light-driven displays, optical storage and optomechanical actuation.

Brinker's group^{63,64} reported the synthesis of photosensitive nanocomposite thin films functionalised with photoresponsive azobenzene-containing organosilane (4-(3-triethoxysilylpropylureido)azobenzene). Azobenzene derivatives were selected because their *trans* \leftrightarrow *cis* isomerisation is UV sensitive. UV irradiation of the *trans* isomer causes transformation to the *cis* isomer. Removal of the UV radiation, heating, or irradiation with a longer wavelength switches the system back to the *trans* form. This isomerisation changes not only the molecular dimension (molecular length of the *cis* isomer is ~ 3.4 Å shorter than that of the *trans* isomer) but also the dipolar moment (0.5–3.1 D) of the organic molecule.

The synthesis^{63,64} scheme employed the azobenzene-modified silane designed to serve as an amphiphilic cosurfactant after hydrolysis of the ethoxy groups. During EISA, the hydrophobic propylureidoazobenzene groups are positioned in the hydrophobic micellar cores, resulting in a highly organised thin film (body-centered cubic mesostructure of *Im3m* space group). At the hydrophilic micellar interface, the hydrophilic $-\text{Si}(\text{OH})_3$ head groups co-condense and co-organise with added silicic acid oligomers. After catalytic or thermally promoted siloxane condensation, azobenzene ligands are anchored to the surfaces of monosized pores and oriented toward the pore interiors (Fig. 9). Subsequent surfactant extraction produces the targeted nanocomposite.

As determined with UV-visible spectroscopy, UV irradiation of the *trans* isomer causes transformation to the *cis* isomer. Removing the UV radiation switches the system back to the *trans* form. As a control experiment, films with the same sol but prepared without the non-ionic Brij56 surfactant were synthesised. In this case, the azobenzene ligands were randomly incorporated in a microporous silica matrix (pore diameter less than 1 nm) and exhibited no detectable photoisomerisation. Similarly, no photoisomerisation for the ordered self-assembled films prior to solvent extraction of the surfactant templates was observed. The pore volume required for photoisomerisation was only obtained upon surfactant removal. These results unambiguously locate the photo-sensitive azobenzene ligands along with surfactant within the uniform nanopores of the self-assembled films.⁶³ These results emphasise the need to accommodate the steric demands of the photoisomerisation process by engineering the pore size and positioning the photoactive species on the pore surfaces.

To demonstrate optical control of mass transport, chronoamperometry experiments were performed using an electrochemical cell working electrode modified with an azobenzene-functionalised nanocomposite membrane (Fig. 10a).⁶⁴ The chronoamperometry experiment used ferrocene dimethanol (FDM) and ferrocene dimethanol diethylene glycol (FDMDG) as an electrochemical probes and provided a measurement of mass transport properties through the nanocomposite hybrid membrane (Fig. 10b). The measurement of mass transport was achieved by monitoring the steady-state oxidative current at constant potential for the reaction taking place on the working electrode surface (made of indium tin oxide, ITO, Fig. 10b). During electrolysis at constant potential, the effective pore size limits the diffusion rate of probing molecules to the electrode surface. Under dark conditions, the azobenzene moieties are predominantly in their extended *trans* form. Upon UV irradiation ($\lambda = 360$ nm), the azobenzene moieties isomerise to the more compact *cis* form which increases the diffusion rate and, correspondingly,

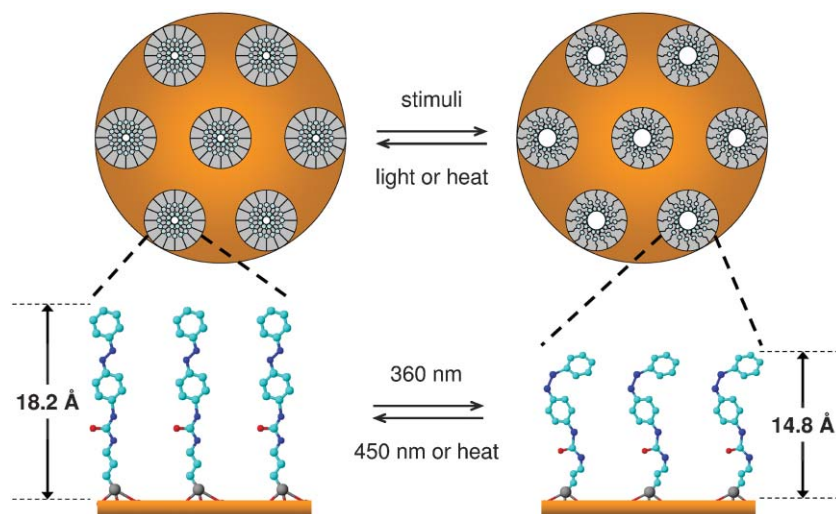


Fig. 9 Photoresponsive nanocomposites prepared by EISA. Atom labels: C: cyan, O: red, N: blue, Si: grey, H atoms are omitted. Adapted from references 63,64.

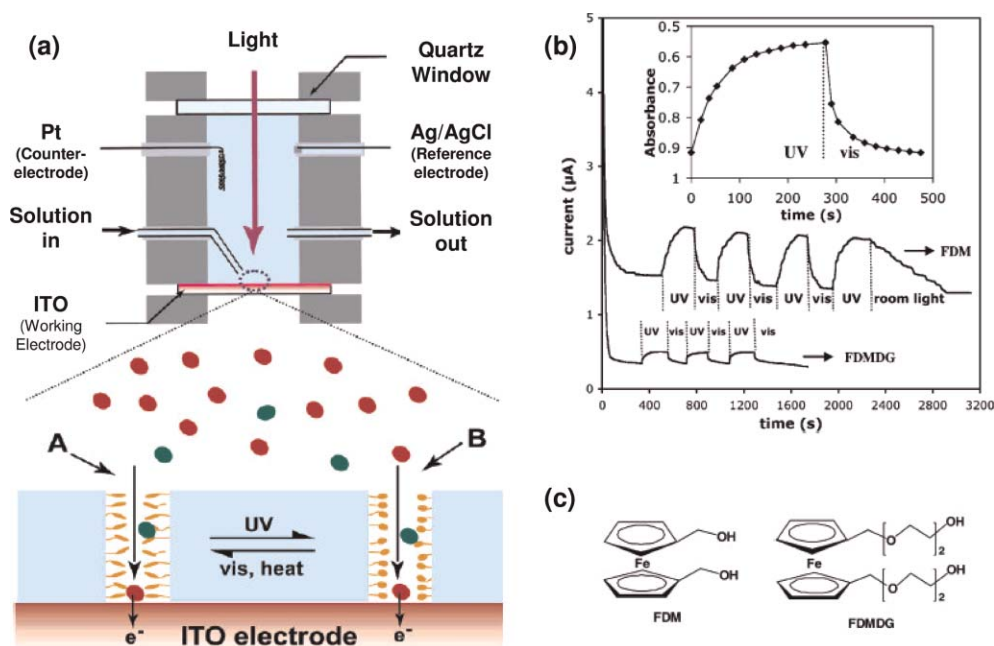


Fig. 10 (a) Schematic drawing of the electrochemical cell (top) and mass transport of probing molecules through the photoresponsive nanocomposite membrane integrated on an ITO electrode (bottom). (A) Diffusion through smaller pores with azobenzene ligands in their *trans* configuration; (B) diffusion through larger pores with azobenzene ligands in their *cis* configuration. Legend: red ovals (FDM or FDMDG, see (c)), green ovals (FDM⁺ or FDMDG⁺), orange ovals (azobenzene in *cis* form), orange elongated ovals (azobenzene in *trans* form). (b) Current–time, $I-t$, behavior of a photoresponsive nanocomposite film under alternate exposure to UV (360 nm) and visible light (435 nm). (Last cycle uses room light, 400–700 nm.) Inset is the absorbance at 356 nm ($\pi-\pi^*$ transition of the *trans* isomer) of the same film immersed in the buffer solution containing 1 mM FDM. (c) Electrochemical probes: ferrocene dimethanol (FDM) and ferrocene dimethanol diethylene glycol (FDMDG).

the oxidative current. Likewise, exposure to visible light ($\lambda = 435$ nm) triggers the reverse *cis*–*trans* isomerisation of the azobenzene moieties, which decreases the current to the pre-UV exposure level. Moreover, it was observed that increasing the volume of the diffusing analyte decreased the overall mass transport, leading to some selectivity for this nanocomposite (Fig. 10b).

3.1.6.5 Controlled release and membranes with switchable permeabilities. Another example of environmentally responsive mesostructured hybrid films is that of polymer/silica nanocomposite¹²⁸ with lamellar mesophases, which swell/deswell upon change of pH or temperature due to the presence of anchored polymers in the interlamellar space. Polymers such as poly(methacrylates) and poly(*N*-isopropylacrylamide) (PNIPAM) show a pronounced response toward changes in pH and temperature, respectively. In water, PNIPAM exhibits a phase transition at the lower critical solution temperature (LCST). This temperature can be controlled through random copolymerisation of NIPAM with methacrylic acid. Below the LCST, the hydrogel incorporates water and swells, whereas water release at higher temperatures causes shrinkage. This property is of interest for controlled release of molecules or for membranes with switchable permeabilities.

Mesoscopically ordered nanocomposite thin films were synthesised, *via* the EISA route, by the incorporation of PNIPAM or its copolymers with dodecyl methacrylate (DM) leading to thin films with silica contents of up to 80%. Solvent evaporation during the deposition step resulted in the

self-assembly of a lamellar mesostructure composed of hundreds of alternating layers of silicic acid and organic species (monomers, coupling agents with alkoxysilane head-groups and a polymerisable double bond, thermal initiators, and surfactants). A heat treatment was employed to initiate the free-radical polymerisation of the confined monomers and promote the condensation of the silica framework.

To study the thermoresponsive behavior, the washed film was immersed in water at temperatures above and below the LCST. Temperature change induced a significant shift of the lamellar d spacing from $d = 3.3$ nm (40 °C) to $d = 5$ nm (30 °C) due to the phase transition of the confined NIPAM/DM copolymers around 30 °C. This lamellar d spacing shift is due to a swelling/deswelling property of the organic part but does not imply any variation of the silica layers thickness. The magnitude of the swelling/deswelling response could be increased by heating and cooling over a larger temperature range (between 10 and 50 °C instead of 30–40 °C). The swelling/deswelling process is reversible and takes *ca.* 5 h, which is comparable to that of bulk systems.

The pH sensitive nanocomposite films containing poly-(dodecyl methacrylate) (PDM) were also studied in water. Poly(methacrylates) are hydrogels showing pronounced changes in chain conformation upon (de)protonation of the carboxyl groups. The authors observed a significant decrease of the lamellar d spacing from $d = 3.3$ nm to $d = 1.9$ nm, with the decrease of the pH (from pH = 9 to 4) probably due to partial hydrolysis of the ester functions of the polymer. In this case too, the swelling/deswelling process was reversible over several cycles.

It is interesting to point out that such PDM/silica mesostructured nanocomposite films also present mechanical properties such as indentation hardness three to seven times greater than amorphous nanocomposites (from 0.1–0.4 GPa to 0.8–1.0 GPa, 1.0 GPa being the indentation hardness measured for rather dense sol–gel silica films). This property is related to the fact that combined organic/inorganic polymerisation results in a laminated structure.⁵²

3.1.6.6 Rapid-prototyping procedures. All the potential applications are dependent on the easiness of processability of such hybrid materials. Brinker's group demonstrated the possibility, using serial rapid printing procedures, to form hierarchically functionalised hybrid mesostructures on several substrates in a few seconds.^{53,124} The rapid-prototyping procedures, *i.e.* micro-pen lithography, ink-jet printing, and dip-coating of patterned self-assembled monolayers, used in this study employ readily available equipment, and provide a link between computer-aided design and self-assembled nanostructures.

By combining self assembly with such processes, the rapid fabrication of hierarchical structures exhibiting form and function on multiple length scales and at multiple locations could be achieved. At the molecular scale, functional organic moieties (*i.e.* $\text{F}_3\text{C}(\text{CF}_2)_5\text{CH}_2\text{CH}_2\text{Si}(\text{OEt})_3/\text{HS}-(\text{CH}_2)_3\text{Si}(\text{OMe})_3/\text{NH}_2-(\text{CH}_2)_3\text{Si}(\text{OMe})_3/\text{dye}-\text{NH}-(\text{CH}_2)_3\text{Si}(\text{OMe})_3$ with dye = 5,6-carboxyfluorescein/ $\text{O}_2\text{N}-\text{C}_6\text{H}_3(\text{NO}_2)-\text{NH}(\text{CH}_2)_3\text{Si}(\text{OEt})_3/(\text{EtO})_3\text{SiCH}_2\text{CH}_2\text{Si}(\text{OEt})_3$) are positioned on pore surfaces by the co-condensation route (“one-pot” synthesis) with TEOS. At the mesoscale, mono-sized pores are

organised into one-, two- or three-dimensional networks, providing size-selective accessibility from the gas or liquid phase. At the macroscale, two-dimensional (2D) arrays and fluidic or photonic systems are designed.

Vital to rapid patterning procedures is the use of stable, homogeneous inks that undergo self-assembly during evaporation to form the desired organically-modified silica–surfactant mesophase. For this purpose, the use of oligomeric silica sols in ethanol/water solvents at a hydronium ion concentration ($[\text{H}_3\text{O}^+] < 0.01 \text{ M}$) adjusted to minimise the siloxane condensation rate is necessary. Indeed, in such conditions facile silica–surfactant self-assembly is possible during the brief time-span of the writing operation (several seconds).

The micro-pen lithography line width, which can vary from micrometres to millimetres, depends on such factors as pen dimension, wetting characteristics, evaporation rate, capillary number and ratio of the rates of ink supply and withdrawal (inlet velocity/substrate velocity). The effect of wetting has been demonstrated by performing micropen lithography (MPL; Fig. 11A) on substrates prepatterned with hydrophobic, hydrophilic or mixed self-assembled monolayers (SAMs). Generally, line widths are reduced by increasing the contact angle and by reducing the pen orifice dimension and inlet/substrate velocity ratio. The versatility of MPL presents two main advantages. Any desired combination of surfactant and functional silane can be used to print selectively different functionalities at different locations. Furthermore, it is possible to use computer-aided design (CAD) to define arbitrary 2D patterns that can be written on different surfaces.

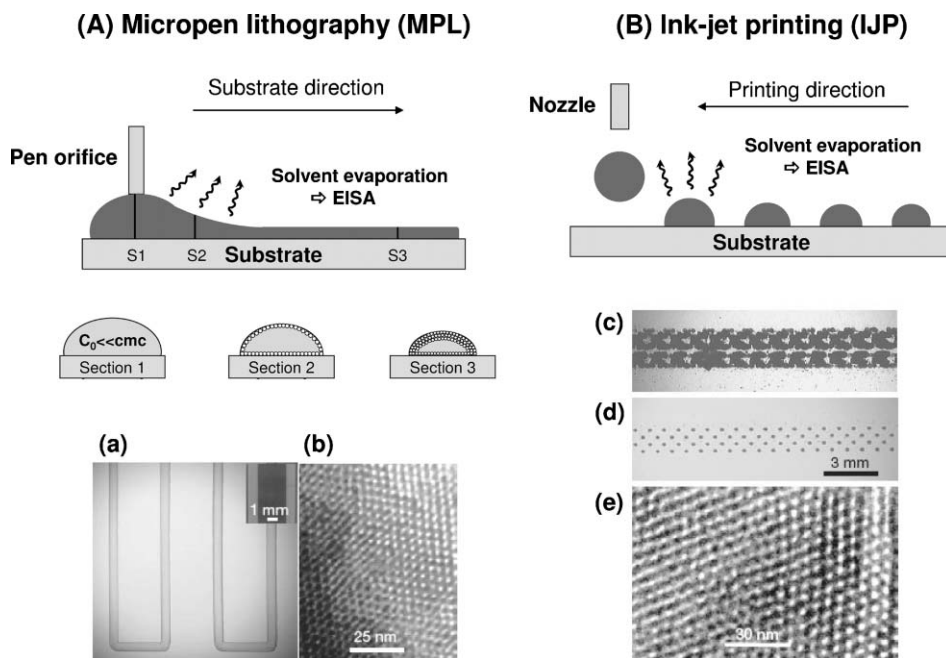


Fig. 11 (A) Principles of combined EISA-MPL patterning. (a) Optical micrograph of patterned rhodamine-B-containing silica mesophase deposited on silicon substrate. Inset is a fluorescence image of rhodamine-B emission demonstrating retention of rhodamine-B functionality. (b) Representative TEM micrograph of a fragment of the patterned rhodamine-containing film corresponding to a [110]-oriented cubic mesophase. (B) Principles of combined EISA-IJP patterning. (c) Optical micrograph of a dot array created by IJP of standard ink (Hewlett-Packard Co.) on a non-adsorbent surface. (d) Optical micrograph of an array of hydrophobic, mesoporous silica dots created by evaporation-induced silica-surfactant self-assembly during IJP on silicon substrate followed by calcination. (e) Representative TEM micrograph of a dot fragment prepared as in (d).

MPL is best suited to write continuous patterns. Patterned macroscopic arrays of discrete mesostructures can be obtained readily by combining EISA with aerosol processing schemes like ink-jet printing (IJP; Fig. 11B). The IJP process dispenses the ink (prepared as for MPL) as monosized, spherical aerosol droplets. Striking the surface, the droplets adopt a new shape that balances surface and interfacial energies. Accompanying evaporation creates within each droplet a gradient in surfactant concentration that drives radially directed silica-surfactant self-assembly inward from the liquid-vapour interface.

MPL and IJP are serial techniques. In situations where it is desirable to create an entire pattern with the same functionality, it might be preferable to employ a parallel technique in which the deposition process occurs simultaneously in multiple locations. This rapid, parallel procedure uses micro-contact printing or electrochemical patterning of hydroxyl- and methyl-terminated self assembled monolayers (SAMs) to define hydrophilic and hydrophobic patterns on the substrate surface. Then, using inks identical to those employed for MPL and IJP, preferential ethanol evaporation during dip-coating enriches the depositing film in water, causing selective de-wetting of the hydrophobic regions and ensuring self-assembly of silica-surfactant mesophases exclusively on the hydrophilic patterns. In this fashion, multiple lines, arrays of dots, or other arbitrary shapes useful for the elaboration of micro-fluidic systems such as pH sensors, can be printed in a few seconds (Fig. 7).

3.2 Post-synthesis of mesostructured hybrid thin films

Another way to synthesise mesoporous hybrid thin films consists of post-grafting organic functions onto the stabilised inorganic walls. So far, modifiers have only been incorporated in silica matrices^{58,125,146–149} as well as in few metal oxide matrices.^{113,150–152} For this latter matrix, the one-pot synthesis approach has not yet been developed.

3.2.1 Post-grafting on metal oxide matrices. Most of the organofunctionalised mesostructured thin films, synthesised either by co-condensation or post-grafting routes, concerned silica-based matrices. Examples of non-silica functionalised mesoporous materials are scarce, even if methods for the synthesis of transition metal oxide films have been developed, either for $\text{MO}_2/\text{M}_2\text{O}_3$ ^{15,153} or mixed oxide frameworks,^{150,151,154} by a general evaporation-induced self-assembly (EISA) procedure. Transition Metal Oxide (TMO) frameworks are interesting for their electronic, mechanical, optical and chemical stability properties. These are particularly interesting because of the electronic properties of the inorganic skeleton, which could be modified by their interaction with included or grafted organic molecules, leading to a great variety of potential applications (magnetic, optoelectronic, and photovoltaic materials). Another potentially interesting application of organically modified mesoporous transition-metal oxides is in controlled-release devices (particularly for non-toxic TiO_2). The feasibility of incorporating organic molecules within mesoporous zirconia thin films by post-synthesis grafting was demonstrated by the Paris group.¹⁵² The

production of hybrid inorganic-organic mesoporous films is often based on the post-synthesis functionalisation of titania or zirconia mesostructures with organic bifunctional molecules F-G, which contain a desired F group and a suitable grafting group (G = phosphonate, phosphate, carboxylate, acetyl acetate, *etc.*) capable of performing complexation of the TM centres (see Table 2).

This procedure leads to highly ordered, non-silica hybrid mesoporous films with organic functions at the pore surface. An important aspect of these films is that the anchoring of the organic groups can be varied, from strong and inert (phosphate, phosphonate) to relatively labile (carboxylate), leading to a great flexibility in the attachment of organic functions, which can be advantageous for several different applications (*e.g.* sensors, controlled release systems). The simplest approach to functionalise mesoporous transition-metal oxide films is the post-grafting route. However, Soler-Illia *et al.*¹¹³ reported recently the one-pot synthesis of highly ordered hybrid mesoporous thin films ($\text{M}_{1-x}(\text{SiR})_x\text{O}_2$) obtained by co-condensation of organotrialkoxysilanes ($\text{R-Si}(\text{OEt})_3$ with R = propylamine, propylthiol and phenyl) with transition metal chloride (MCl_4 with M = Zr or Ti). As the chemical bonds between probes and the matrix involve metal chelating groups, the direct incorporation of the probes in the starting sol has to be carefully controlled in order to avoid hindrance of the mesostructuration process. However, the post-functionalisation of such thin films is not straightforward, and particular attention has to be paid to aspects such as surface chemistry, diffusion within pores, dissolution, *etc.* Another important issue is the integrity of modified mesoporous transition-metal oxides (MTMOs) under solvent flux (*i.e.*, function leaching), due to the fact that functions are grafted via coordination or ionic-covalent bonds to the pore wall.

In these studies,^{113,150–152} mesoporous films with a 2D hexagonal or cubic mesostructure were prepared by EISA, using a triblock copolymer (Pluronic F127) or Brij-58 [$\text{C}_{16}\text{H}_{33}(\text{CH}_2\text{CH}_2\text{O})_{20}\text{OH}$] templates.^{82,90,152} The films were thermally stabilised by several post-synthesis treatments until complete removal of the template. A typical functionalisation experiment was performed by dipping the calcined mesoporous film, previously rinsed with ethanol, into a continuously-stirring solution of the chosen molecule in THF, acetone, or water.

Kinetics experiments showed that molecule incorporation occurs in two steps and that over 80% of the incorporated functional groups enter the pore system within 5 min. The remaining 20% are gradually incorporated and saturation is reached between 60 and 120 min. Moreover, the function incorporation depends on the mesostructure; cubic 3D mesostructures are more accessible than their 2D hexagonal counterparts.

The trends issuing from leaching experiments demonstrate that the anchoring strength follows the complexation strength of the grafting group, that is, $\text{R-O-PO}_3^{2-} \sim \text{R-PO}_3^{2-} > \text{dicarboxylate} > \text{carboxylate}$, for groups with high solubility in the leaching solvent. An interesting characteristic of these hybrid mesoporous films is that, in contrast to the irreversible grafting observed in mesoporous hybrid silica, anchoring groups with different strengths can be selected to obtain a wide

Table 2 Modifiers and properties of resultant thin films mesophases

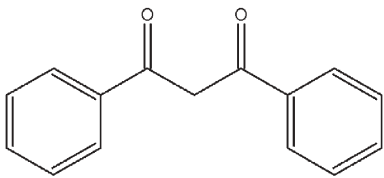
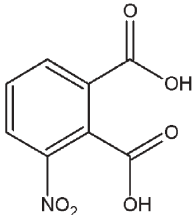
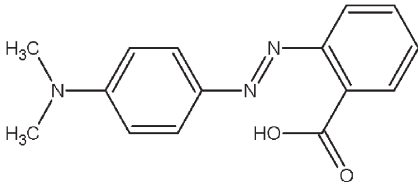
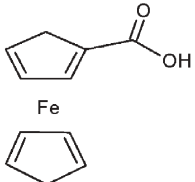
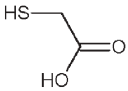
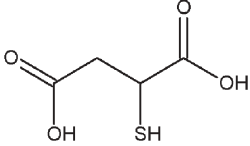
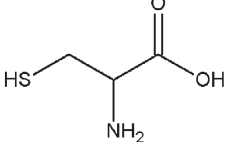
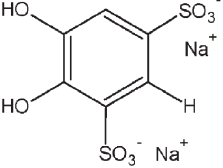
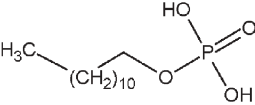
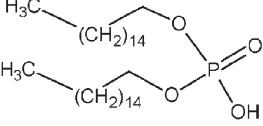
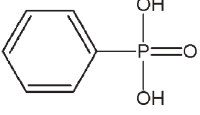
Functional organosilanes	Experimental conditions and results	Properties/applications and references
41) Dibenzoylmethane	ZrCl ₄ , Brij 58; 2D hexagonal	Hydrophobic ¹⁵²
		
42) 3-Nitrophthalic acid	ZrCl ₄ /TiCl ₄ , F127; cubic, 2D hexagonal	¹⁵⁰
		
43) Methyl Red	ZrCl ₄ , Brij 58; 2D hexagonal	pH sensitive ¹⁵²
		
44) Ferrocenecarboxylic acid	ZrCl ₄ , Brij 58; 2D hexagonal	Redox properties ¹⁵²
		
45) Thioglycolic acid	ZrCl ₄ /TiCl ₄ , F127; cubic, 2D hexagonal	¹⁵¹
		
46) Mercaptosuccinic acid	ZrCl ₄ /TiCl ₄ , F127; cubic, 2D hexagonal	^{150,151}
		
47) Cysteine	ZrCl ₄ /TiCl ₄ , F127; cubic, 2D hexagonal	¹⁵⁰
		

Table 2 Modifiers and properties of resultant thin films mesophases (*Continued*)

Functional organosilanes	Experimental conditions and results	Properties/applications and references
48) Disodium 1,2-dihydroxybenzene-3,5-disulfonate	ZrCl ₄ /TiCl ₄ , F127; cubic, 2D hexagonal	¹⁵⁰
		
49) Monododecylphosphate	ZrCl ₄ /TiCl ₄ , F127; cubic, 2D hexagonal	Sensors, controlled release devices, sorption ^{150,151}
		
50) Dihexadecylphosphate	ZrCl ₄ /TiCl ₄ , F127; cubic, 2D hexagonal	Sensors, controlled release devices, sorption ¹⁵⁰
		
51) Phenylphosphonic acid	ZrCl ₄ /TiCl ₄ , F127; cubic, 2D hexagonal ZrCl ₄ , Brij 58; 2D hexagonal	Sensors, controlled release devices, sorption ^{150,151} Hydrophobic ¹⁵²
		

variety of responses, from strongly attached functions to functions that can be liberated by external stimuli.

Following these authors,^{150,151} it can be concluded that two main limitations to (large) functionalisers incorporation arise: (i) pore accessibility (related to the symmetry and connectivity of the pore array) and (ii) transport within the pore system. The latter factor can be explained in terms of molecule diffusion (with the limitations imposed by the diffusion of a molecule commensurate with the pore size) and also molecule/wall interactions. Interactions have been recently identified as a key factor in the modification of small-molecule diffusion coefficients within the pore system of functionalised mesoporous silica.^{155,156} Earlier work in post-functionalised 2D hexagonal silica powders demonstrated that organosilane functional groups were concentrated on the outer surface and near the pore openings; this is possible when the grafting reaction is fast (relative to transport to the pore interior) and almost irreversible, which should be the case for silanes post-grafted onto silica pore surfaces.³⁵ In fact, the transport of the grafting molecule to the inner pores of MTMOs could follow a sequence of adsorption–desorption–diffusion. Hence, a higher complexation ability of the grafting group should result in slower incorporation of the organic function. The solvent also plays an important role, particularly favoring the desorption step. For example, the leaching rates of mercaptosuccinic acid are higher at low pH, where the acid is fully protonated, due to the fact that carboxylate anchoring groups become more labile at low pH. Indeed, the presence of protons facilitates the

cleavage by water of the anchored carboxylates. This feature can be used in controlled delivery devices, where the release of an anchored drug can be triggered by the external pH.

MTMO surfaces can be flexibly modified with various functional groups which can be retained or liberated depending on the external conditions (pH, solvent, *etc.*). This is a substantial difference when compared to the strong silane bonding to silica, which leads to an almost “irreversible” functionalisation. Functionalised pores are further accessible to other molecules (solvent, fluorescent probes) or ions (*i.e.*, Hg(II)), opening the way for sensor or sorption applications.

3.2.2 Post-grafting on silica-based matrices. As described previously, the most commonly employed method to functionalise mesostructured silica thin films is the one-pot synthesis. However, some studies employing post-functionalisation have been reported.^{58,146–149} Typically, after a thermal treatment, which allows both good consolidation of the inorganic network and removal of the template, thin films were stirred in dry toluene solution containing organotrialkoxysilane under refluxing conditions. The reaction time was varied from 6 to 24 h. Finally, thin films were washed with solvent and dried at low temperature. An alternative route to post-functionalise thin films before the calcination step *via* a vapour infiltration technique was also recently reported.¹⁴⁷ According to the authors, hydrophobic organosiloxane molecules (Me_nSi(OEt)_{4–n}) penetrated into mesostructured silica films and were incorporated into the mesochannel silica walls.

The post-functionalisation presents several advantages compared to co-condensation route: (i) treatment at high temperatures (around 400 °C) results in a highly condensed inorganic network and increases the stability of thin films, (ii) the functionalisation takes place only in the pores of films, (iii) no phase transition can happen with the incorporation of the probes, implying a conservation of the initial mesophase.¹⁴⁶ However, as stated previously post-grafting may result in an inhomogeneous coating of the pore surface by the organosilanes (localised near the pore openings) leading to restriction¹⁴⁹ (ink bottle pores) or to a total blocking of the porosity.¹⁴⁶

This post-functionalisation procedure was used to develop lead(II) electrochemical sensors,¹⁴⁹ chemical ammonia and water sensors based on dielectric responses of films,⁵⁸ and as a mould for the synthesis of gold nanowires.¹⁴⁸

Yantasee *et al.*¹⁴⁹ tested the applicability of the thiol-functionalised mesoporous silica (SH-FMS) thin film as an electrode sensing layer. Mesoporous thin films were spin-coated onto the bare surface of a gold microelectrode array microchip. After the calcination step, the modified microelectrode was grafted with 3-mercaptopropyltrimethoxysilane. The process of absorptive stripping voltammetry detection of Pb(II) using the SH-FMS thin-film electrode involves several steps. The preconcentration step results in an accumulation of Pb(II) ions on the surface of the nanopores by complexation with the thiol groups of the surface. During the detection step accumulated Pb(II) ions desorb from the FMS surface in an acidic medium (*e.g.* 0.1 M HNO₃) and diffuse to the surface of the gold electrode. The authors demonstrated that functionalised mesoporous thin films with high binding site density, due to the high surface area of the mesoporous structure, lead to high sensitivity and large dynamic range for metal ion sensing.

Domansky *et al.*⁵⁸ post-functionalised mesoporous silica films with hexadimethylsilazane. By measuring the dielectric constant and the dissipation factor of functionalised thin films exposed to water vapour, ammonia, and methane, they observed that the films presented good sensitivity to both water vapour and ammonia in air. It is interesting to point out that, in contrast to most chemical sensors, these films were not functionalised with groups for specific molecular recognition.

Gu *et al.*¹⁴⁸ developed a three step strategy to incorporate highly dispersed gold nanowires into the pore channels of mesoporous thin films. After synthesis and extraction of the template, the pore surface was modified with aminopropyltrimethoxysilane. The H₂AuCl₄ salt was introduced into films *via* a neutralisation reaction. Following a reduction procedure, Au nanowires were formed within the thin films. It should be emphasised that using this strategy, films not only served as a confined template, a function for traditional wet impregnation method, but also as a reactor for the neutralisation reaction.

4 Conclusion

Hybrid organic–inorganic materials are increasingly taking their position in the free spaces left between inorganic chemistry, polymer chemistry, organic chemistry, and biology. This land of research, initially worked on by the sol–gel

community, is at present thriving with the appearance of a new class of mesoscopic hybrid structures and the strong input of bioinspired materials scientists.¹⁵⁷ These periodically organised mesoporous hybrids, which can be shaped as films or coatings through a large set of versatile processes, present important advantages because they facilitate integration and miniaturisation of the devices (nanomaterials, nanotechnologies) and their hybridisation afford a direct connection between the inorganic, organic and biological worlds. Hybrid organic–inorganic mesoporous thin films are promising but, considering developments and applications they are still in their infancy. Some promising properties concerning optical sensing, low-*k* dielectrics, photonic, molecular valves or nano-gates, controlled release, switchable membranes have already been investigated but they only represent the tip of the iceberg.

In particular, many multiscale structured hybrids (from nanometer to the millimeter scale) thin films will appear in the near future, opening a land of opportunities for designing new materials. More developments are expected within the next few years with the involvement of organic and organometallic chemists who will design new precursors to enable better tuning of the material functionality.

The outlook for nano-sciences in the 21st century is indeed promising because many of these hybrid films will be developed as smart materials or integrated in devices with applications satisfying socio-economical demands in energy, environment, information, health and medicine. Selective separation, adsorption, catalysis, sensing, biosensing, photonic or optical devices, fuel cell and battery photovoltaic cells, membranes with coupled properties (sensing, catalysis, separation, *etc.*) are but a few examples.

Acknowledgements

This work was performed in the frame of the FAME European Network of Excellence.

References

- 1 D. Avnir, D. Levy and R. Reisfeld, *J. Phys. Chem.*, 1984, **88**, 5956.
- 2 C. J. Brinker and G. W. Scherer, *Sol–Gel Science*, Academic Press, San Diego, 1990.
- 3 H. Schmidt, A. Kaiser, H. Patzelt and H. Scholze, *J. Phys.*, 1982, **12**, 275.
- 4 J. Livage, M. Henry and C. Sanchez, *Prog. Solid State Chem.*, 1988, **18**, 259.
- 5 C. Sanchez and F. Ribot, *New J. Chem.*, 1994, **18**, 1007.
- 6 U. Schubert, N. Husing and A. Lorenz, *Chem. Mater.*, 1995, **7**, 2010.
- 7 P. Judenstein and C. Sanchez, *J. Mater. Chem.*, 1996, **6**, 511.
- 8 D. A. Loy and K. J. Shea, *Chem. Rev.*, 1995, **95**, 1431.
- 9 R. J. P. Corriu, *C. R. Acad. Sci. Paris, Sér. IIC*, 1998, **1**, 83.
- 10 C. Sanchez, F. Ribot and B. Lebeau, *J. Mater. Chem.*, 1999, **9**, 35.
- 11 E. Bourgeat-Lamy, *J. Nanosci. Nanotechnol.*, 2002, **2**, 1.
- 12 C. Sanchez, G. J. d. A. A. Soler-Illia, F. Ribot, T. Lalot, C. R. Mayer and V. Cabuil, *Chem. Mater.*, 2001, **13**, 3061.
- 13 *Functional Hybrid Materials*, ed. P. Gómez-Romero and C. Sanchez, Wiley-VCH, Weinheim, 2003.
- 14 C. Sanchez, B. Lebeau, F. Chaput and J. P. Boilot, *Adv. Mater.*, 2003, **15**, 1969.
- 15 G. J. d. A. A. Soler-Illia, C. Sanchez, B. Lebeau and J. Patarin, *Chem. Rev.*, 2002, **102**, 4093.
- 16 C. Sanchez, G. J. D. A. A. Soler-Illia, F. Ribot and D. Grosso, *C. R. Chim.*, 2003, **6**, 1131.

- 17 K. Moller and T. Bein, *Chem. Mater.*, 1998, **10**, 2950.
- 18 A. Stein, B. J. Melde and R. C. Schroden, *Adv. Mater.*, 2000, **12**, 1403.
- 19 A. Sayari and S. Hamoudi, *Chem. Mater.*, 2001, **13**, 3151.
- 20 R. Burch, N. Cruise, D. Gleeson and S. C. Tsang, *Chem. Commun.*, 1996, 951.
- 21 T. Maschmeyer, F. Rey, S. Gopinathan and J. M. Thomas, *Nature*, 1995, **378**, 159.
- 22 D. Brunel, A. Cauvel, F. Fajula and F. Di Renzo, *Stud. Surf. Sci. Catal.*, 1995, **97**, 173.
- 23 D. Brunel, *Microporous Mesoporous Mater.*, 1999, **27**, 329.
- 24 D. Brunel, A. C. Blanc, A. Galarneau and F. Fajula, *Catal. Today*, 2002, **73**, 139.
- 25 S. L. Burkett, S. D. Sims and S. Mann, *Chem. Commun.*, 1996, 1367.
- 26 C. E. Fowler, S. L. Burkett and S. Mann, *Chem. Commun.*, 1997, 1769.
- 27 D. J. Macquarrie, *Chem. Commun.*, 1996, 1961.
- 28 M. H. Lim, C. F. Blanford and A. Stein, *J. Am. Chem. Soc.*, 1997, **119**, 4090.
- 29 F. Babonneau, L. Leite and S. Fontlupt, *J. Mater. Chem.*, 1999, **9**, 175.
- 30 L. Mercier and T. J. Pinnavaia, *Chem. Mater.*, 2000, **12**, 188.
- 31 Y. F. Lu, H. Y. Fan, N. Doke, D. A. Loy, R. A. Assink, D. A. LaVan and C. J. Brinker, *J. Am. Chem. Soc.*, 2000, **122**, 5258.
- 32 T. Asefa, M. J. MacLachan, N. Coombs and G. A. Ozin, *Nature*, 1999, **402**, 867.
- 33 S. Inagaki, S. Guan, T. Ohsuna and O. Terasaki, *Nature*, 2002, **416**, 304.
- 34 B. J. Melde, B. T. Holland, C. F. Blanford and A. Stein, *Chem. Mater.*, 1999, **11**, 3302.
- 35 M. H. Lim and A. Stein, *Chem. Mater.*, 1999, **11**, 3285.
- 36 G. Ogawa, *Curr. Opin. Colloid Interface Sci.*, 2001, **4**, 209.
- 37 H. Yang, N. Coombs, Ö. Dag, I. Sokolov and G. A. Ozin, *J. Mater. Chem.*, 1997, **7**, 1755.
- 38 A. S. Brown, S. A. Holt, T. Dam, M. Trau and J. W. White, *Langmuir*, 1997, **13**, 6363.
- 39 S. H. Tolbert, T. E. Schäffer, J. Feng, P. K. Hansma and G. D. Stucky, *Chem. Mater.*, 1997, **9**, 1962.
- 40 J. E. Martin, M. T. Anderson, J. Odinek and P. Newcomer, *Langmuir*, 1997, **13**, 4133.
- 41 H. Yang, N. Coombs, I. Sokolov and G. Ozin, *Nature*, 1996, **381**, 589.
- 42 S. Schacht, Q. Huo, I. Voigt-Martin, G. D. Stucky and F. Schuth, *Science*, 1996, **273**, 768.
- 43 H. Yang, A. Kuperman, N. Coombs, S. Mamiche-Afara and G. Ozin, *Nature*, 1996, **379**, 703.
- 44 I. Aksay, M. Trau, S. Manne, I. Honma, N. Yao, L. Zhou, P. Fenter, P. Eisenberger and S. Gruner, *Science*, 1996, **273**, 892.
- 45 G. Ogawa, *Chem. Commun.*, 1996, 1149.
- 46 C. J. Brinker, Y. Lu, A. Sellinger and H. Fan, *Adv. Mater.*, 1999, **11**, 579.
- 47 S. Besson, C. Ricolleau, T. Gacoin, C. Jacquiod and J. P. Boilot, *J. Phys. Chem. B*, 2000, **104**, 12095.
- 48 D. Y. Zhao, P. D. Yang, N. Melosh, Y. L. Feng, B. F. Chmelka and G. Stucky, *Adv. Mater.*, 1998, **10**, 1380.
- 49 Y. Lu, R. Ganguli, C. A. Drewien, M. T. Anderson, C. J. Brinker, W. Gong, Y. Guo, H. Soye, B. Dunn, M. H. Huang and J. I. Zink, *Nature*, 1997, **389**, 364.
- 50 D. A. Doshi, N. K. Huesing, M. C. Lu, H. Y. Fan, Y. F. Lu, P. K. Simmons, B. G. Potter, A. J. Hurd and C. J. Brinker, *Science*, 2000, **290**, 107.
- 51 D. Grosso, A. R. Balkenende, P.-A. Albouy, M. Lavergne, L. Mazerolles and F. Babonneau, *J. Mater. Chem.*, 2000, **10**, 2085.
- 52 A. Sellinger, P. M. Weiss, N. Anh, Y. Lu, R. A. Assink, W. Gong and C. J. Brinker, *Nature*, 1998, **394**, 256.
- 53 H. Y. Fan, Y. F. Lu, A. Stump, S. T. Reed, T. Baer, R. Schunk, L. V. Perez, G. P. Lopez and C. J. Brinker, *Nature*, 2000, **405**, 56.
- 54 Y. Lu, H. Fan, A. Stump, T. L. Ward, T. Rieker and C. J. Brinker, *Nature*, 1999, **398**, 223.
- 55 C. T. Kresge, M. E. Leonowicz, W. J. Roth, J. C. Vartuli and J. S. Beck, *Nature*, 1992, **359**, 710.
- 56 T. Clark, J. D. Ruiz, H. Y. Fan, C. J. Brinker, B. I. Swanson and A. N. Parikh, *Chem. Mater.*, 2000, **12**, 3879.
- 57 Y. F. Lu, Y. Yang, A. Sellinger, M. C. Lu, J. M. Huang, H. Y. Fan, R. Haddad, G. Lopez, A. R. Burns, D. Y. Sasaki, J. Shelnutt and C. J. Brinker, *Nature*, 2001, **410**, 913.
- 58 K. Domansky, J. Liu, L. Q. Wang, M. H. Engelhard and S. Baskaran, *J. Mater. Res.*, 2001, **16**, 2810.
- 59 G. Wirnsberger, B. J. Scott and G. D. Stucky, *Chem. Commun.*, 2001, 119.
- 60 L. Nicole, C. Boissière, D. Grosso, P. Hesemann, J. Moreau and C. Sanchez, *Chem. Commun.*, 2004, 2312.
- 61 C. Y. Tsai, *J. Membr. Sci.*, 2000, **169**, 255.
- 62 P. Yang, G. Wirnsberger, H. C. Huang, S. R. Cordero, M. D. McGehee, B. Scott, T. Deng, G. M. Whitesides, B. F. Chmelka, S. K. Buratto and G. D. Stucky, *Science*, 2000, **287**, 465.
- 63 N. G. Liu, Z. Chen, D. R. Dunphy, Y. B. Jiang, R. A. Assink and C. J. Brinker, *Angew. Chem., Int. Ed.*, 2003, **42**, 1731.
- 64 N. G. Liu, D. R. Dunphy, P. Atanassov, S. D. Bunge, Z. Chen, G. P. Lopez, T. J. Boyle and C. J. Brinker, *Nano Lett.*, 2004, **4**, 551.
- 65 R. D. Miller, *Science*, 1999, **286**, 421.
- 66 H. Fan, H. R. Bentley, K. R. Kathan, P. Clem, Y. Lu and C. J. Brinker, *J. Non-Cryst. Solids*, 2001, **285**, 79.
- 67 D. Grosso, F. Cagnol, G. J. d. A. A. Soler-Illia, E. L. Crepaldi, H. Amenitsch, A. Brunet-Bruneau, A. Bourgeois and C. Sanchez, *Adv. Funct. Mater.*, 2004, **14**, 309.
- 68 J. S. Beck, J. C. Vartuli, W. J. Roth, M. E. Leonovicz, C. T. Kresge, K. D. Schmitt, C. T. W. Chu, D. H. Olson and E. W. Sheppard, *J. Am. Chem. Soc.*, 1992, **114**, 10834.
- 69 A. Galarneau, D. A. Lerner, M. F. Ottaviani, F. D. Renzo and F. Fajula, *Stud. Surf. Sci. Catal.*, 1998, 1998.
- 70 J. Frash, B. Lebeau, M. Soular and J. Patarin, *Langmuir*, 2000, **16**, 9049.
- 71 D. Grosso, F. Babonneau, P.-A. Albouy, H. Amenitsch, A. R. Balkenende, A. Brunet-Bruneau and J. Rivory, *Chem. Mater.*, 2002, **14**, 931.
- 72 C. Boissière, A. Larbot, C. Bourgaux, E. Prouzet and C. A. Bunton, *Chem. Mater.*, 2001, **13**, 3580.
- 73 Q. Huo, D. I. Margolese, U. Ciesla, D. G. Demuth, P. Feng, T. E. Gier, P. Sieger, A. Firouzi, B. F. Chmelka, F. Schuth and G. D. Stucky, *Chem. Mater.*, 1994, **6**, 1176.
- 74 C. C. Landry, S. H. Tolbert, K. W. Gallis, A. Monnier, G. D. Stucky, P. Norby and J. C. Hanson, *Chem. Mater.*, 2001, **13**, 1600.
- 75 S. H. Tolbert, C. C. Landry, G. D. Stucky, B. F. Chmelka, P. Norby, J. C. Hanson and A. Monnier, *Chem. Mater.*, 2001, **13**, 2247.
- 76 J. Patarin, B. Lebeau and R. Zana, *Curr. Opin. Colloid Interface Sci.*, 2002, **7**, 107.
- 77 P. Innocenzi, P. Falcato, D. Grosso and F. Babonneau, *J. Phys. Chem. B*, 2003, **107**, 4711.
- 78 The CMC for the hybrid system may not be the one for the surfactant alone.
- 79 D. Grosso, F. Babonneau, G. J. d. A. A. Soler-Illia, P.-A. Albouy and H. Amenitsch, *Chem. Commun.*, 2002, 748.
- 80 F. Cagnol, D. Grosso, G. J. d. A. A. Soler-Illia, E. L. Crepaldi, F. Babonneau, H. Amenitsch and C. Sanchez, *J. Mater. Chem.*, 2003, **13**, 61–66.
- 81 D. Grosso, F. Babonneau, C. Sanchez, I. G. Soler, E. L. Crepaldi, P. A. Albouy, H. Amenitsch, A. R. Balkenende and A. Brunet-Bruneau, *J. Sol-Gel Sci. Technol.*, 2003, **26**, 561.
- 82 E. L. Crepaldi, G. J. d. A. A. Soler-Illia, D. Grosso, F. Cagnol, F. Ribot and C. Sanchez, *J. Am. Chem. Soc.*, 2003, **125**, 9770.
- 83 D. Grosso, A. R. Balkenende, P.-A. Albouy, A. Ayrat, H. Amenitsch and F. Babonneau, *Chem. Mater.*, 2001, **13**, 1848.
- 84 D. Kundu, H. S. Zhou and I. Honma, *J. Mater. Sci. Lett.*, 1998, **17**, 2089.
- 85 F. Schuth, *Chem. Mater.*, 2001, **13**, 3184.
- 86 E. L. Crepaldi, I. G. Soler, A. Bouchara, D. Grosso, D. Durand and C. Sanchez, *Angew. Chem., Int. Ed.*, 2003, **42**, 347.
- 87 D. Grosso, I. G. Soler, E. L. Crepaldi, F. Cagnol, C. Sinturel, A. Bourgeois, B. A. Brunet, H. Amenitsch, P. A. Albouy and C. Sanchez, *Chem. Mater.*, 2003, **15**, 4562.

- 88 D. Grosso, C. Boissiere, B. Smarsly, T. Brezesinski, N. Pinna, P. A. Albouy, H. Amenitsch, M. Antonietti and C. Sanchez, *Nature Mater.*, 2004, **3**, 787.
- 89 Z. L. Hua, J. L. Shi, L. Wang and W. H. Zhang, *J. Non-Cryst. Solids*, 2001, **292**, 177.
- 90 D. Grosso, I. G. Soler, F. Babonneau, C. Sanchez, P. A. Albouy, B. A. Brunet and A. R. Balkenende, *Adv. Mater.*, 2001, **13**, 1085.
- 91 M. H. Lim, C. F. Blanford and A. Stein, *Chem. Mater.*, 1998, **10**, 467.
- 92 R. J. P. Corriu, C. Hoarau, A. Mehdi and C. Reye, *Chem. Commun.*, 2000, 71.
- 93 Q. M. Zhang, K. Ariga, A. Okabe and T. Aida, *J. Am. Chem. Soc.*, 2004, **126**, 988.
- 94 B. Alonso, P. A. Albouy, D. Durand and F. Babonneau, *New J. Chem.*, 2002, **26**, 1270.
- 95 B. Alonso, A. R. Balkenende, P. A. Albouy, H. Amenitsch, M. N. Rager and F. Babonneau, *J. Sol-Gel Sci. Technol.*, 2003, **26**, 587.
- 96 F. K. de Theije, A. R. Balkenende, M. A. Verheijen, M. R. Baklanov, K. P. Mogilnikov and Y. Furukawa, *J. Phys. Chem. B*, 2003, **107**, 4280.
- 97 J. I. Jung, J. Y. Bae and B. S. Bae, *J. Mater. Chem.*, 2004, **14**, 1988.
- 98 F. Cagnol, D. Grosso and C. Sanchez, *Chem. Commun.*, 2004, 1742.
- 99 A. Gibaud, J. F. Bardeau, M. Dutreilh-Colas, M. Bellour, V. V. Balasubramanian, A. Robert, A. Mehdi, C. Reye and R. J. Corriu, *J. Mater. Chem.*, 2004, **14**, 1854.
- 100 Y. Yang, Y. F. Lu, M. C. Lu, J. M. Huang, R. Haddad, G. Xomeritakis, N. G. Liu, A. P. Malanoski, D. Sturmayer, H. Y. Fan, D. Y. Sasaki, R. A. Assink, J. A. Shelnutt, S. F. van, G. P. Lopez, A. R. Burns and C. J. Brinker, *J. Am. Chem. Soc.*, 2003, **125**, 1269.
- 101 B. Smarsly, G. Garnweitner, R. Assink and C. J. Brinker, *Prog. Org. Coat.*, 2003, **47**, 393.
- 102 P. Innocenzi, P. Falcaro, S. Schergna, M. Maggini, E. Menna, H. Amenitsch, I. J. A. A. Soler, D. Grosso and C. Sanchez, *J. Mater. Chem.*, 2004, **14**, 1838.
- 103 N. G. Liu, K. Yu, B. Smarsly, D. R. Dunphy, Y. B. Jiang and C. J. Brinker, *J. Am. Chem. Soc.*, 2002, **124**, 14540.
- 104 K. Yu, B. Smarsly and C. J. Brinker, *Adv. Funct. Mater.*, 2003, **13**, 47.
- 105 N. G. Liu, R. A. Assink, B. Smarsly and C. J. Brinker, *Chem. Commun.*, 2003, 1146.
- 106 P. N. Minoofar, R. Hernandez, S. Chia, B. Dunn, J. I. Zink and A.-C. Franville, *J. Am. Chem. Soc.*, 2002, **124**, 14388.
- 107 R. Hernandez, A.-C. Franville, P. Minoofar, B. Dunn and J. I. Zink, *J. Am. Chem. Soc.*, 2001, **123**, 1248.
- 108 P. Minoofar, R. Hernandez, A. C. Franville, S. Y. Chia, B. Dunn and J. I. Zink, *J. Sol-Gel Sci. Technol.*, 2003, **26**, 571.
- 109 N. A. Melosh, P. Lipic, F. S. Bates, F. Wudl, G. D. Stucky, G. H. Fredrickson and B. F. Chmelka, *Macromolecules*, 1999, **32**, 4332.
- 110 H. Li, L. Fu, F. Liu, S. Wang and H. Zhang, *New J. Chem.*, 2002, **26**, 674.
- 111 O. Dag, I. C. Yoshina, T. Asefa, M. J. MacLachlan, H. Grondey, N. Coombs and G. A. Ozin, *Adv. Funct. Mater.*, 2001, **11**, 213.
- 112 E. M. Wong, M. A. Markowitz, S. B. Qadri, S. Golledge, D. G. Castner and B. P. Gaber, *J. Phys. Chem. B*, 2002, **106**, 6652.
- 113 G. Soler-Illia, P. C. Angelome and P. Bozzano, *Chem. Commun.*, 2004, 2854.
- 114 V. Goletto, V. Dagry and F. Babonneau, *Mater. Res. Soc. Symp. Proc.*, 1999, **576**, 229.
- 115 R. Nagarajan, *Curr. Opin. Colloid Interface Sci.*, 1997, **2**, 282.
- 116 R. Nagarajan, *Curr. Opin. Colloid Interface Sci.*, 1996, **1**, 391.
- 117 D. Desplandier-Giscard, A. Galarneau, F. Di Renzo and F. Fajula, *Stud. Surf. Sci. Catal.*, 2001, **135**, 6P27.
- 118 R. A. Kumpf and D. A. Dougherty, *Science*, 1993, **261**, 1708.
- 119 K. S. Kim, J. Y. Lee, S. J. Lee, T.-K. Ha and D. H. Kim, *J. Am. Chem. Soc.*, 1994, **116**, 7399.
- 120 J. Israelachvili, D. J. Mitchell and B. W. Ninham, *J. Chem. Soc., Faraday Trans.*, 1976, **72**, 1525.
- 121 S. Besson, T. Gacoin, C. Ricolleau, C. Jacquiod and J. P. Boilot, *J. Mater. Chem.*, 2003, **13**, 404.
- 122 E. M. Wong, M. A. Markowitz, S. B. Qadri, S. L. Golledge, D. G. Castner and B. P. Gaber, *Langmuir*, 2002, **18**, 972.
- 123 N. G. Liu, R. A. Assink and C. J. Brinker, *Chem. Commun.*, 2003, 370.
- 124 H. Fan, S. Reed, T. Baer, R. Schunk, G. P. Lopez and C. J. Brinker, *Microporous Mesoporous Mater.*, 2001, **44-45**, 625.
- 125 C. M. Yang, A. T. Cho, F. M. Pan, T. G. Tsai and K. J. Chao, *Adv. Mater.*, 2001, **13**, 1099.
- 126 B. Lebeau, C. E. Fowler, S. R. Hall and S. Mann, *J. Mater. Chem.*, 1999, **9**, 2279.
- 127 P. N. Minoofar, B. S. Dunn and J. I. Zink, *J. Am. Chem. Soc.*, 2005, **127**, 2656.
- 128 G. Garnweitner, B. Smarsly, R. Assink, W. Ruland, E. Bond and C. J. Brinker, *J. Am. Chem. Soc.*, 2003, **125**, 5626.
- 129 C. Rottman, M. Ottolenghi, R. Zusman, O. Lev, M. Smith, G. Gong, M. L. Kagan and D. Avnir, *Mater. Lett.*, 1992, **13**, 293.
- 130 A. Lobnik, I. Oehme, I. Murkovic and O. S. Wolfbeis, *Anal. Chim. Acta*, 1998, **367**, 159.
- 131 L. Yang and S. S. Saavedra, *Anal. Chem.*, 1995, **65**, 1307.
- 132 J. Stary and E. Hladky, *Anal. Chim. Acta*, 1963, **28**, 227.
- 133 K. Maex, M. R. Baklanov, D. Shamiryan, F. Iacopi, S. H. Brongersma and Z. S. Yanovitskaya, *J. Appl. Phys.*, 2003, **93**, 8793.
- 134 M. H. Huang, H. M. Soye, B. S. Dunn and J. I. Zink, *Chem. Mater.*, 2000, **12**, 231.
- 135 A. C. Franville, B. Dunn and J. I. Zink, *J. Phys. Chem. B*, 2001, **105**, 10335.
- 136 M. H. Huang, B. S. Dunn and J. I. Zink, *J. Am. Chem. Soc.*, 2000, **122**, 3739.
- 137 M. H. Huang, B. S. Dunn, H. Soye and J. I. Zink, *Langmuir*, 1998, **14**, 7331.
- 138 B. J. Scott, M. H. Bartl, G. Wirsberger and G. D. Stucky, *J. Phys. Chem. A*, 2003, **107**, 5499.
- 139 B. Lebeau, C. Guermeur and C. Sanchez, *Mater. Res. Soc. Symp. Proc.*, 1994, **346**, 315.
- 140 F. Bentivegna, M. Canva, P. Georges, A. Brun, F. Chaput, L. Malier and J. P. Boilot, *Appl. Phys. Lett.*, 1993, **62**, 1721.
- 141 P. Innocenzi, G. Brusatin, H. A. P. Eckert and M. A. P. Ward, *Chem. Mater.*, 2001, **13**, 3126.
- 142 P. Innocenzi, G. Brusatin, M. Guglielmi, R. Signorini, M. Meneghetti, R. Bozio, M. Maggini, G. Scorrano and M. Prato, *J. Sol-Gel Sci. Technol.*, 2000, **19**, 263.
- 143 P. Innocenzi, G. Brusatin, M. Guglielmi, R. Signorini, R. Bozio and M. Maggini, *J. Non-Cryst. Solids*, 2000, **265**, 68.
- 144 R. Signorini, M. Meneghetti, R. Bozio, M. Maggini, G. Scorrano, M. Prato, G. Brusatin, P. Innocenzi and M. Guglielmi, *Carbon*, 2000, **38**, 1653.
- 145 G. Brusatin, P. Innocenzi, M. Guglielmi, R. Signorini and R. Bozio, *Nonlinear Opt.*, 2001, **27**, 259.
- 146 N. Petkov, S. Mintova, B. Jean, T. Metzger and T. Bein, *Mater. Sci. Eng. C: Biomimet. Supramol. Syst.*, 2003, **23**, 827.
- 147 S. Tanaka, J. Kaihara, N. Nishiyama, Y. Oku, Y. Egashira and K. Ueyama, *Langmuir*, 2004, **20**, 3780.
- 148 J. L. Gu, J. L. Shi, Z. Hua, L. M. Xiong, L. X. Zhang and L. Li, *Chem. Lett.*, 2005, **34**, 114.
- 149 W. Yantasee, Y. Lin, X. Li, G. E. Fryxell, T. S. Zemanian and V. V. Viswanathan, *Analyst*, 2003, **128**, 899.
- 150 P. C. Angelome and I. G. Soler, *Chem. Mater.*, 2005, **17**, 322.
- 151 P. C. Angelome, B. S. Aldabe, M. E. Calvo, E. L. Crepaldi, D. Grosso, C. Sanchez and I. G. Soler, *New J. Chem.*, 2005, **29**, 59.
- 152 E. L. Crepaldi, G. J. d. A. A. Soler-Illia, D. Grosso, P.-A. Albouy and C. Sanchez, *Chem. Commun.*, 2001, 1582.
- 153 G. J. d. A. A. Soler-Illia, E. L. Crepaldi, D. Grosso and C. Sanchez, *Curr. Opin. Colloid Interface Sci.*, 2003, **8**, 109.
- 154 G. Soler-Illia, E. L. Crepaldi, D. Grosso and C. Sanchez, *J. Mater. Chem.*, 2004, **14**, 1879.
- 155 E. W. Hansen, F. Courivaud, A. Karlson, S. Kolboe and M. Stöcker, *Microporous Mesoporous Mater.*, 1998, **22**, 309.
- 156 F. Stallmach, A. Graser, J. Karger, C. Krause, M. Jeschke, U. Oberhagemann and S. Spange, *Microporous Mesoporous Mater.*, 2001, **44**, 745.
- 157 C. Sanchez, H. Arribart and M. M. G. Guille, *Nature Mater.*, 2005, **4**, 277.
- 158 M. Ogawa and T. Kikuchi, *Adv. Mater.*, 1998, **10**, 1077.
- 159 A. Shimojima and K. Kuroda, *Angew. Chem., Int. Ed.*, 2003, **42**, 4057.